Universidad de Sevilla

Bachelor's Degree in Physics

Beam Loss Monitors
in the Large Hadron Collider

Author:

Sara Morales Vigo

US Tutors:

Jorge Fernández Berni

Rocío del Río

CERN Supervisor:

Belén Salvachúa

June 18, 2020

Contents

Acknowledgements

First of all, I would like to thank my tutors, Jorge and Rocío, for contributing with their knowledge and expertise to the preparation of this work. From the very beginning they made me feel completely free to conduct my research as I wanted, encouraging me to expand my horizons, develop a scientific thinking and pursue excellence. Our exchanges were always rewarding and helpful. I hope that this thesis reflects at least a tiny fraction of the passion and the effort they put in everything they do.

It goes without saying that this would not have been possible if it had not been for Belén, who gave me the opportunity to take part in this amazing project with her and taught me almost everything that is included in this work. I think I never told you personally how lucky I feel to have had you as my master and partner in crime during these months. All I can say is thank you for everything you have done for me. This thesis is also a result of your work. I cannot wait to start our next project.

I would also like to thank my colleagues from the BE-BI-BL section for making me feel at home and turning my stay at CERN into one of the best experiences I ever had. I am really looking forward to seeing you again and sharing the daily coffee meetings and lunch breaks in R3 with you. Special mention should be given to Christos and Ewald, who had a smile for me every time I had questions about the BLM system or I wanted to discuss my results.

Of course, I cannot miss the person with whom I shared the office for more than one year and who had to put up with my stories and bad jokes on a daily basis. Thank you, Lorenzo, for being the best office mate I could have ever imagined.

André is my greatest discovery at CERN and my biggest support. No one knows me like you do. Thank you for being always there for me and for making my days happier. It would not have been the same without you. I am really fortunate to have you by my side.

Last, but not least, I would like to thank the most supportive family in the world, Antonio, Carmen y Antoñito. Despite the distance, they always find the right words to cheer me up and make my days. My biggest wish is to be with them by the day of the presentation.

Abstract

The LHC at CERN is the largest and most powerful particle accelerator ever built. It accelerates protons and ions at high speeds, close to the speed of light, and collides them with the purpose of recreating the conditions which could be present seconds after the Big Bang occurred.

The high energy and intensity of the LHC particle beams makes them highly destructive for the machine components. Only the loss of a small fraction of the beam particles could produce a quench in the superconducting magnets or damage detector equipment. Therefore, it is essential to install a safety system which monitors the beam losses during operation of the LHC and triggers the beam dump when the losses exceed certain predetermined thresholds.

These tasks are performed by the LHC BLM system, with more than 4000 detectors covering the 27 km LHC circumference. As the BLM system is a fundamental element concerning the LHC machine protection, it is important to analyze its signal continuously in order to detect possible damage or degradation of its components, potentially caused by the high-radiation environment in which they are installed.

The main objective of this work is to give an overview on both the LHC and BLM system, followed by the analysis of the BLM noise signal and the BLM integrated dose during Run 2 (2015-2018). These analysis were performed using tools created as part of this Bachelor's Thesis. The results obtained were fundamental to determine that for the moment no BLM system limitations due to radiation effects are to be expected in future operation periods of the LHC.

List of Acronyms

ADC   Analogue-to-Digital Converter

ALICE   A Large Ion Collider Experiment

ALPHA   Antihydrogen Laser PHysics Apparatus

ATLAS   A Toroidal LHC ApparatuS

ASACUSA Atomic Spectroscopy And Collisions Using Slow Antiprotons

BETS   Beam Energy Tracking System

BIS   Beam Interlock System

BLECF   Beam Loss Electronic Current-to-Frequency

BLECS   Beam Loss Electronic Combiner and Survey

BLETC   Beam Loss Electronic Threshold Comparator

BLM   Beam Loss Monitoring

CALS   CERN Accelerator Logging Service

CERN   Conseil Européen pour la Recherche Nucléaire

CFC   Current-to-Frequency Converter

CMS   Compact Muon Solenoid

DAC   Digital-to-Analogue Converter

DS   Dispersion Suppressor

GUI   Graphical User Interface

IC   Ionization Chamber

IP   Insertion Point

IR   Insertion Region

ISOLDE   Isotope Separator On Line DEvice

LEP   Large Electron-Positron collider

LHC   Large Hadron Collider

LHCb   Large Hadron Collider beauty

LIC   Little Ionization Chamber

LINAC 2   Linear Accelerator 2

LINAC 4   Linear Accelerator 4

LSS   Long Straight Section

MD   Machine Devlopment

n_TOF   Neutron Time-Of-Flight

NXCALS   NeXt CERN Accelerator Logging Service

Op-Amp   Operational Amplifier

PS   Proton Synchrotron

PSB   Proton Synchrotron Booster

RF   Radiofrequency

RS   Running Sum

SC   Synchrocyclotron

SEM   Secondary Emission Monitor

SPS   Super Proton Synchrotron

TCLA   Target Collimator, Long Absorber

TCP   Target Collimator, Primary

TCS   Target Collimator, Secondary

TCT   Target Collimator, Tertiary

TS   Technical Stop

1 Introduction

1.1 CERN, European Organization for Nuclear Research

The European Organization for Nuclear Research, also known by its acronym CERN, is the largest particle physics laboratory in the world. Its origin dates back to the end of the II World War, after which European science was no longer world-class. With the aim of increasing international scientific collaboration, as well as becoming again an example of excellence and top-level research, some scientists imagined creating an European atomic physics laboratory. Among the different proposals that were made, the one which suggested focusing on fundamental physics research, with absolutely no military goals, was selected [1].

The convention establishing CERN was ratified on 29 September 1954 by 12 European countries under the name Conseil Européen pour la Recherche Nucléaire, from which its acronym derives. It was decided that the organization would sit astride the Franco-Swiss border near Geneva, following its strategic location in central Europe, Swiss neutrality during the war and its tradition hosting numerous international organisations.

Among the significant achievements made by the laboratory throughout its history, some deserve to be highlighted.[1] The operation of CERN machines and experiments has been key to important discoveries in the field of particle physics from its early beginnings. After all, CERN's first accelerator, the SC, which started to operate in 1957, could detect for the first time, already in 1958, a rare pion decay that had remained undetected for other machines of similar energy and intensity from the rest of laboratories in the world [2].

CERN's most recent achievement was the observation of a new particle consistent with the Higgs boson. This was possible through the operation of the **LHC**, the world's largest and most powerful particle accelerator, which has been performing proton-proton collisions since 2008. On July 4, 2012, the LHC experiments ATLAS and CMS presented evidence in the LHC data of the mentioned particle. The 2013 Nobel Prize in Physics was awarded

---

[1]The research conducted at CERN has not only contributed to discoveries in the fields of nuclear of particle physics, but also to the development of engineering and computing techniques. One example is the World Wide Web, invented at CERN in 1989 by British scientist Tim Berners-Lee.

jointly to François Englert and Peter Higgs, which had predicted theoretically the existence of the particle.

CERN is currently run by 23 member states and it employs approximately 2 500 staff members. They are in charge of the design, construction and operation of the accelerator infrastructure. CERN comprises a large community of users with more than 12 000 scientists coming from institutes all around the world. They are responsible for the preparation and operation of the experiments, as well as for the analysis of the data gathered from them. CERN personnel has teams contributing to the experiments. Additionally, approximately 800 fellows, 600 students and 1 300 associates also take part in CERN's activities. This creates a network of more than 17 500 people from different nationalities who work together with the same purpose: push the boundaries of human knowledge and understand what the universe is made of and how it works. Although CERN's main focus is Particle Physics, its Physics program covers other topics such as Nuclear or High-Energy Physics, including studies of Antimatter and even cosmic rays effects.

1.2   Introduction to Accelerator Physics

When two particles that are sufficiently energetic collide, the well-known Einstein's equation $E = mc^2$ comes into play. This equation is a representation of the mass-energy equivalence, according to which matter is a concentrated form of energy, and the two are interchangeable. The energy of the collision is transformed into matter and as a result new massive particles are generated. The majority of these particles decay immediately into lighter particles after they are created, and they can be identified in different layers of particle detectors. The study of the results of these collisions can help us discover new particles, measure their properties and have a better understanding of what matter is and how it can be related to the origins of the universe.

An **accelerator** is a machine that accelerates and steers electrically charged particles making use of electromagnetic fields. The accelerated particles are then directed onto a target or collided with other particles. An accelerator which also performs head-on collisions between

the particles is called a **collider**. The advantage of performing head-on collisions is that the collision energy is higher, as the energies of the two particles are added together. Accelerators and colliders are intended to recreate the conditions which could be present seconds after the Big Bang occurred. There are circular and linear accelerators.

In an accelerator the charged particles are accelerated inside **RF cavities**, metallic chambers containing alternating electric fields supplied by an RF power generator. RF cavities are molded a specific size and shape so that electromagnetic waves become resonant and build up inside the cavity. The field in an RF cavity is made to oscillate (switch direction) at a given frequency, so that the beam particles always see an accelerating electric field both when they arrive and leave the cavity. Therefore, timing the arrival of particles is crucial for them to receive this electrical impulse [3]. A more graphical explanation can be found in Figure A.1 in Appendix A. As a consequence of this RF acceleration scheme, beams of particles are not continuous in modern accelerators. They circulate in well-defined packs called **bunches**. Their length and distance between them depend on the RF system characteristics.

The RF cavities have essentially two functions, depending on the energy of the particles:

- During acceleration to the top energy, they deliver RF power to the beam.

- Once the accelerator is at full energy, they keep the bunches tight. The ideally timed particle, with exactly the right energy, will see zero accelerating voltage. Protons with slightly different energies arriving earlier or later will be accelerated or decelerated so that they stay close to the energy of the ideal particle.

Without any other force involved, the particles would drift apart and their momentum would carry them in a straight line. For this reason, **dipole magnets** are employed to bend the trajectory of the particles in circular accelerators. Furthermore, **quadrupole magnets** are employed to focus the particle beams. They have four magnetic poles arranged symmetrically around the beam pipe to squeeze the beam either vertically or horizontally. On the other hand, a linear accelerator is mostly composed of accelerating structures, as there is no need to bend the particles in their trajectories along the machine.

A remarkable difference between the two is that in a circular accelerator the energy of the particles is increased with each turn, while in a linear accelerator they only benefit from a single acceleration pass. However, the energy of the particles cannot be increased infinitely, as the higher it is, the more powerful the magnetic fields to keep the particles in their orbit. The nominal energy of an accelerator defines the maximum energy a particle could acquire when circulating inside it, and it is a trade-off between its size, radius of curvature (if it is circular) and cost, among others.[2]

Accelerators and colliders are built to study processes which require high energies and are hard to obtain. When two bunches cross, only a small amount of particles collide. The **luminosity** of a collider is a quantity which is related to the probability of performing a particle collision. It depends on machine and beam parameters, such as the number of particles in each bunch, the frequency of complete turns around the ring, the number of bunches and the beam cross-section. In order to achieve higher luminosity values, the density of the bunches is maximized by increasing the number of particles per bunch and decreasing the beam size. The inverse femtobarn (fb^{-1}) is the unit used to measure integrated luminosity, or the cumulative number of potential collisions over a given period of time.

1.3   CERN Accelerator Complex

The CERN Accelerator Complex is a succession of machines, experiments and accelerators with increasing beam energies. To date, it is composed of eight accelerators, two decelerators, the transfer lines which interconnect them and numerous facilities hosting experiments aimed at covering topics in the fields of Particle Physics (e.g., ATLAS, CMS), Nuclear Physics (ISOLDE) and Antimatter (ALPHA, ASACUSA), among others. Part of them sit on the surface, but the largest ones are located underground. An overview of the Accelerator Complex is presented in Figure 1.

Some of these accelerators supply particles to the experiments and others are used as injectors, accelerating particles for larger accelerators. The majority of them perform both

---

[2]When the energy that a particle acquires in an accelerator is mentioned, it refers to its kinetic energy.
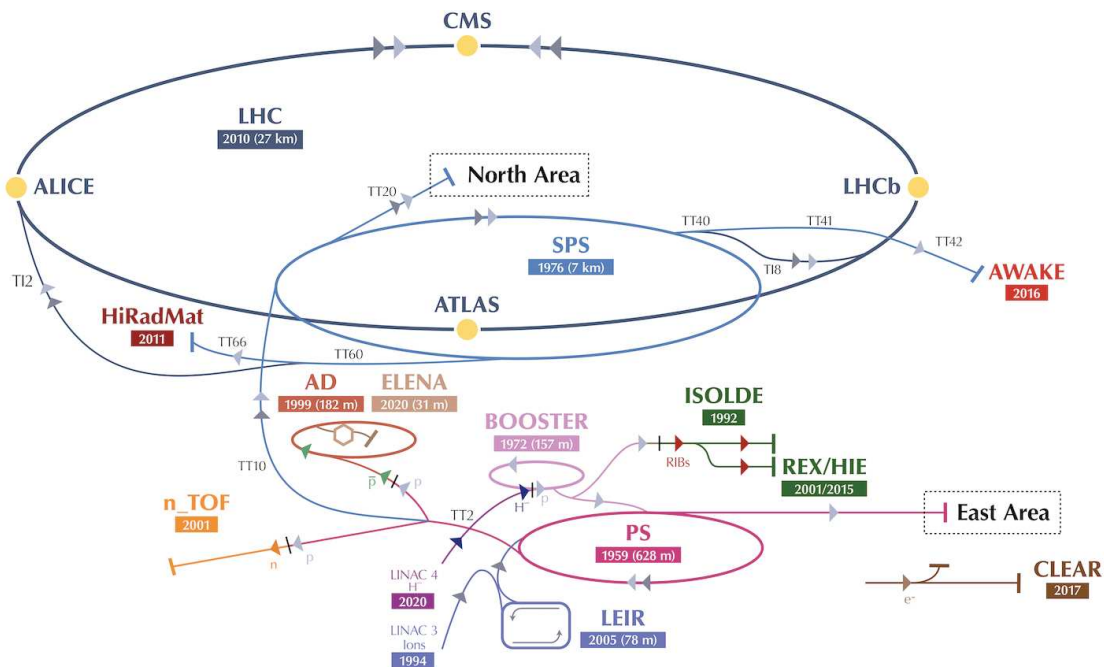
Figure 1: CERN Accelerator Complex. The LHC is the last ring (dark blue line) in a complex chain of particle accelerators [4].

tasks. Despite the fact that the CERN Accelerator Complex accelerates protons most of the time during operation, some runs are dedicated to ions of lead, argon or xenon atoms.

The LHC is a circular particle accelerator and collider, the largest in the world and hence in the Accelerator Complex. It has a 27-km circumference and it accelerates particles up to a nominal (design) energy of 7 TeV, which corresponds to 99.9999964 % of the speed of light, before taking them into collision.[3]

However, the particles do not start being accelerated from zero in the LHC. They are injected with a certain energy which they have already acquired during their journey through a chain of one linear and three circular accelerators. As most of the LHC runs are dedicated to protons, a focus on their path in the Accelerator Complex is presented [5].

---

[3]According to Einstein's theory of Special Relativity, the total energy of a particle can be expressed as $E = mc^2 = \gamma m_0 c^2$, where m_0 is the mass of the particle at rest and γ the Lorentz factor, defined as $\gamma = \frac{1}{\sqrt{1 - \frac{v^2}{c^2}}}$. Taking into account that the total energy of a particle can also be expressed as $E = E_0 + E_k$, being E_0 the energy at rest and E_k the kinetic energy of the particle, and combining the expressions presented, the fraction between the speed of a particle and the speed of light can be obtained as $\frac{v}{c} = \sqrt{1 - (\frac{1}{1 + \frac{E_k}{m_o c^2}})^2}$.

The source of the protons is a bottle of hydrogen gas. The gas is passed through an electric field which separates electrons and protons, leaving only the latter to enter into LINAC 2, a linear accelerator in which the protons reach an energy of 50 MeV, which corresponds to 31.4 % of the speed of light. LINAC 2 has recently been replaced by LINAC 4, which will start operating after the long shutdown (2019-2020). It will accelerate negative hydrogen ions to 160 MeV, which corresponds to 52.0 % of the speed of light [6].

With this new configuration, the hydrogen ions are stripped of their two electrons during injection from LINAC 4 into the PSB to leave only protons. It is the first circular accelerator of the injection chain, where the particles reach an energy of 1.4 GeV, equivalent to 91.6 % of the speed of light. It is also the accelerator where the beam is divided into bunches.

The bunches of protons are injected in the PS, where the protons reach an energy of 25 GeV, which corresponds to 99.93 % of the speed of light. These three accelerators are located on the surface.

They are followed by the SPS, which is located 60 m underground [7]. Inside this accelerator, the particles are accelerated to 450 GeV, 99.9998 % of the speed of light.

In these accelerators bunches of particles circulate in only one direction. It is during the extraction from the SPS and the injection in the LHC via two transfer lines that the two beams of particles which travel in the LHC in opposite directions are generated.

A total of 1.51×10^{20} protons were accelerated in the complex in 2017, from which the LHC used less than 0.084 %. Most of these particles are used by the ISOLDE and n_TOF facilities, 61.45 % and 14.30 % respectively. Approximately 14 % of the particles are used for operating tests (MDs)[4] or are not used at all (beam dumps, losses, etc.) [8].

The LHC has been performing proton acceleration and proton-proton collisions during Run 1 (2011-2013) and Run 2 (2015-2018), experiencing an increasing performance through the years. This includes a beam energy of 6.5 TeV, with up to 2 556 bunches per beam and, on average, 1.15×10^{11} particles per bunch, achieved during Run 2 [9].[5]

---

[4]The MDs are planned periods scheduled for studies on beam adjustment and for testing new components.

[5]Even though the design beam energy of the LHC is 7 TeV, Run 2 (2015-2018) was scheduled to run at a lower energy, 6.5 TeV, in order to optimise the time needed to train the magnets before the start of the operation period and allow a higher number of particle collisions for physics research [10].

Under these conditions, the total energy in each beam at top energy (6.5 TeV) is approximately 300 MJ,[6] which is approximately as energetic as a 400-ton train, like the French TGV, travelling at 140 km/h. Only the loss of a small fraction of the beam particles could damage the accelerator or the detector equipment. Safe operation of the LHC requires correct operation of several systems specially designed for machine protection. Some of them are aimed at monitoring the beam characteristics, such as beam size, beam position or beam lifetime.

Driven by these concerns, a **BLM system** was installed in the LHC. It actively prevents the machine from beam losses by triggering a beam dump signal when the measured losses exceed certain predetermined thresholds [11]. The BLM signal can also be used to assess the total prompt radiation dose received by machine components as well as the residual dose expected from irradiated machine elements.

The BLM system is a fundamental element concerning the LHC machine protection. In order to detect possible damage or degradation of the BLM components, it is essential to continuously monitor its signal and its variations as a function of time and detector location.

An overview of the LHC general structure and systems is presented with the purpose of understanding its complexity and heterogeneity, as well as identifying the regions which are most affected by beam losses and should be followed up with the help of its BLM system.

The main components of the LHC BLM system are also described with a special focus on the BLM signal generation and the variations in location and time it presented during Run 2. This includes an analysis on the BLM noise signal which is essential for the detection of failures or degradation of the system, often caused by radiation effects.

Additionally, an analysis of the BLM system integrated dose is shown indicating the location of the most radiated BLM detectors and how their received dose changes with machine parameters such as luminosity or beam intensity.

Following this review, a study of the total dose effects on the signal of the most radiated BLM detectors is presented with the aim of determining if a BLM system limitation due to radiation effects is to be expected in future operation periods of the LHC.

---

[6]This result can be obtained with a simple calculation: E_{beam} = 2556 bunches × 1.15 × 10^{11} particles per bunch × 6.5 TeV per particle.

2 LHC

As mentioned in previous sections, the LHC is the largest infrastructure of CERN's accelerator complex. Its name comes from its size (approximately 27 km in circumference), and the fact that it is an accelerator and collider of protons or ions, which are hadrons. Two particle beams travel in opposite directions in the same cryostat and collide at four specific points, where the beams intersect.

The LHC is composed of two rings, one per beam injected from the SPS. Ring 1 corresponds to Beam 1, which circulates clockwise, and Ring 2 corresponds to Beam 2, which circulates counter-clockwise in a top view. Both beams circulate inside the beam pipes which are kept at ultrahigh vacuum to prevent the collision of the beam particles with the particles present in the air. The rings are 27-km long and located inside a tunnel 100 m underground, which was initially excavated for the construction of the LEP, an accelerator and collider that was operating for 11 years before it was dismantled in 2 000 for the construction of the LHC [12].

The LHC is designed and built to accelerate particles up to a nominal beam energy of 7 TeV. The fact that the beams of particles travel in opposite directions inside the accelerator is key to obtain head-on collisions events with centre of mass energies of up to 14 TeV, as the energies of the particles are added up.

Actually, these energies are not so impressive in absolute terms, if we take into account that the top energy that one proton would acquire in the LHC is similar to the energy of motion of a small insect. What makes it special is that this energy is concentrated into a space approximately a million million times smaller, narrower than a human hair.

2.1 LHC Superconducting Magnets

Dipole electro-magnets are used to bend the trajectory of the particles along circular accelerators. The higher the energies of the particles, the more powerful the magnetic fields need to be in order to keep their orbits inside the beam pipes. The challenge for the LHC magnet system is to make the most profitable use of the existing LEP tunnel. Aiming at

beam energies of up to 7 TeV inside the LEP tunnel implies a dipole field of 8.33 T, 100 000 times more powerful than the Earth's magnetic field. Thus, a current of 11 850 A is required to flow in the dipoles [13].

In order to reach and maintain the required current to produce these strong magnetic fields, superconducting coils are employed in the LHC magnets. Superconductivity is a special state that some materials enter when they are kept below a certain characteristic temperature. Under this state they can conduct electrical currents with almost zero electrical resistance. The use of superconducting coils in the LHC magnets allows to maintain very high currents with considerably lower energy losses. These superconducting magnets rely on Nb-Ti cables which are cooled down to a temperature of 1.9 K.

The two beams of equally charged particles require opposite magnetic dipole fields, as they travel in opposite directions. There is not enough room for separate rings of magnets in the LEP tunnel. Therefore, the LHC uses twin bore magnets which consist of two sets of coils and beam channels within the same mechanical structure and cryostat. The particle beams circulate in two different beam pipes most of the time. They only intersect in four points, where four large detectors are placed to study the results of the particle collisions. A picture of the LHC tunnel with a 3D recreation of the cross section of a dipole is presented in Figure A.2 in Appendix A. Additionally, a picture of a slice through a LHC superconducting dipole and a LHC superconducting quadrupole is presented in Figure A.3 in Appendix A.

2.2   LHC Layout

The LHC layout is presented in Figure 2. The LHC is not completely circular, it has eight **arcs** and eight **IRs**. Each IR consists of a **LSS** and two (one at each end) transition regions called **DSs** [14]. Each LSS is approximately 528-m long and can serve as an experimental or utility insertion. The middle of an IR is called its **IP**. In the IRs where the two LHC beams cross over, the IP indicates the point where the two LHC beams intersect. Those IRs are called **experimental IRs**. There are four experimental IRs, and the different LHC large experimental caverns are located in each of them: ATLAS, ALICE, CMS and LHCb.
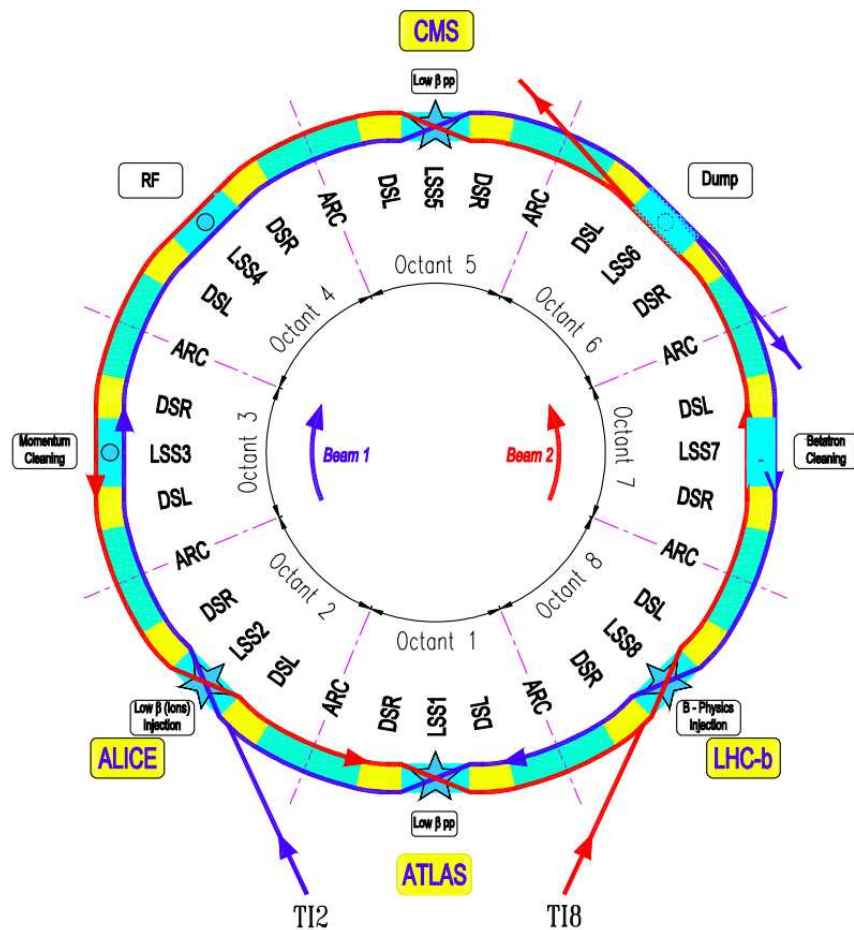
Figure 2: LHC Layout. Beam 1 and 2 are indicated in blue and red respectively. TI2 and TI8 are the transmission lines which inject the beams from the SPS. The collision points are indicated with stars [5].

Following this geometrical structure, the two particle beams have separate magnetic fields and beam pipes in the main arcs and share an approximately 130-m long common beam pipe only at the experimental IRs.

For practical reasons and organizational purposes, the LHC layout can be divided and described in **octants**. An octant starts in the centre of an arc and continues to the centre of the next arc clockwise. Therefore, the IP of an IR corresponds to the middle of the octant where it is located. IP1 is in the middle of IR1 and Octant 1, and it corresponds to the collision point of the ATLAS experiment. The rest of the IPs and octants are numbered from 1 to 8 following the direction of Beam 1 (clockwise).

10

2.2.1   IR1, IR2, IR5 and IR8: Experimental IRs

The ATLAS, ALICE, CMS and LHCb experiments are located in IR1, IR2, IR5 and IR8, respectively. These experiments consist in particle detectors placed around the point where the beams intersect and the particles collide. ATLAS and CMS are high-luminosity experiments. LHCb is a low-luminosity experiment for B-physics, a specialty within the field of Particle Physics concerned with studying the properties of B hadrons, hadrons containing at least one bottom quark. ALICE is dedicated to ion operations.

In these IRs, before the particle beams enter the detectors, just prior to collision, another type of magnet is used to squeeze the beam particles closer together to increase the chances of collisions with particles coming from the opposite direction, and therefore, the luminosity [15]. Three quadrupoles are used to create a system called an inner triplet. There are eight inner triplets, two of which are located at each of the four aforementioned large LHC detectors. Inner triplets tighten the beam, making it 12.5 times narrower, from 0.2-mm transversal size, down to 16 μm across. As well as sharing the beam pipe, the two counter-rotating beams share the triplets in the experimental IRs.

Moreover, magnets are also needed to deviate the trajectory of the beams and cross them at the collision points. The separation/recombination magnets are special dipole magnets responsible for these beam crossings in the experimental IRs. They are located left and right from the triplet magnets.[7] They bring the two beams onto a colliding orbit at the interaction point and then separate them again beyond the collision point. They are also used as in several insertions where they are needed to change the beam separation from the nominal 194 mm in the LHC arcs.

Apart from the ALICE and LHCb experiments, IR2 and IR8 also contain the injection systems for Beam 1 and Beam 2 coming from the SPS.

---

[7]The words "right" and "left" here describe the position in the tunnel relative to an observer inside the ring looking out.

2.2.2   IR4: RF Systems

As shown in Figure 2, IR4 contains two RF systems, one independent system for each LHC beam, as well as some of the LHC beam instrumentation. The RF system is designed so that each particle gains an energy of 485 keV with each passage through the cavities. For injection energy each RF system has to provide approximately 8 MV, while at top energy up to 16 MV are required. Each RF system is composed of eight cavities, each delivering up to 2 MV at top energy, equivalent to an accelerating field of 5 MV/m. The 450 GeV injection energy of the particles rises to 6.5 TeV in approximately 20 min, bunches having passed through the RF cavities more than 10 million times. During acceleration to the top energy, the field in the LHC magnets increases as the energy of the particles does. As explained in Section 1.2, once the top energy is reached, the main role of the LHC RF cavities is to keep the approximately 2 556 proton bunches tight, controlling the bunch length.

2.2.3   IR3 and IR7: Collimation Systems

During operation of any accelerator, individual particles can suffer a deviation from their foreseen path and end up hitting the beam pipes, machine elements or even the inner part of a detector. This incident is called a **beam loss**.

The unprecedented amount of energy stored in the LHC beams makes them highly destructive. Only the loss of a small amount of the beam particles could damage machine elements or produce a **quench** in the superconducting magnets.[8] At top energy, losses on the level of $30\,\mathrm{mJ/cm^3}$, induced by a local transient loss of 4×10^7 protons would produce a quench on the superconducting magnet coil [5].

Beam dynamics processes caused by single particle dynamics and collective effects may cause some particles to increase their transverse oscillation amplitudes or suffer a variation in their energies. These effects can arise from the electromagnetic interaction of the beam particles among themselves, with their environment and with the other beam, among other

---

[8]A magnet quench is defined as the loss of the superconducting state in the coils of a superconducting magnet when it is heated above its characteristic temperature. This phenomenon can occur accidentally due to energy deposition from beam losses in the superconducting coils.

sources. The fact that the bunches of particles have a finite length and are not singular is also key to understand the difference in energy among the particles in a bunch. Even though the RF pulse is synchronized with the arrival of the particles to the cavities, only those located in the center of the bunch will receive the exact amount of energy required for beam acceleration. The rest of the particles in the bunch will circulate in the LHC rings with slightly lower or higher energies. As a consequence of this, the deviation they receive due to the magnetic fields in the dipoles will not be ideal either, resulting in a transverse offset.

Particles with transverse oscillation amplitudes or energy deviations (longitudinal oscillation amplitudes) significantly larger than those of the reference particle are referred to as **beam halo** particles. One can distinguish between betatron and off-momentum halos, which are formed in the case of larger-than-nominal transverse amplitudes or energy errors, respectively. In order to guarantee the LHC machine protection, beam losses should be avoided during operation. However, they cannot be completely suppressed. There will always be a so-called "primary beam halo". Various beam loss mechanisms can cause outwards drifts of halo particles if there is no mechanism to safely intercept them [16].

In order to clean these halo particles, and considering the high intensity LHC beams and the associated high loss rates of protons, a powerful **collimation system** is required. The general purpose of a collimation system is to dispose, safely, efficiently and in a controlled way, of beam losses that would otherwise occur at sensitive locations or on accelerator equipment which is not designed to face these losses. Designing a collimation system involves setting up an arrangement of collimators which ensures that losses in superconducting magnets remain below the quench limits for all types of loss rates. The key elements and arrangement of the LHC multi-stage collimation system are shown in Figure 3.

Beam collimation is achieved by placing blocks of material, the collimator jaws, close to the circulating beams, to constrain the betatron amplitudes of stray particles outside the core of the beam and absorb them. Collimation of off-momentum tails is achieved in a similar way as for betatron tails, by placing collimators at locations of high dispersion, where the particle's transverse offset caused by energy shifts is higher. They are preferably placed in warm regions, as far as possible from superconducting magnets.
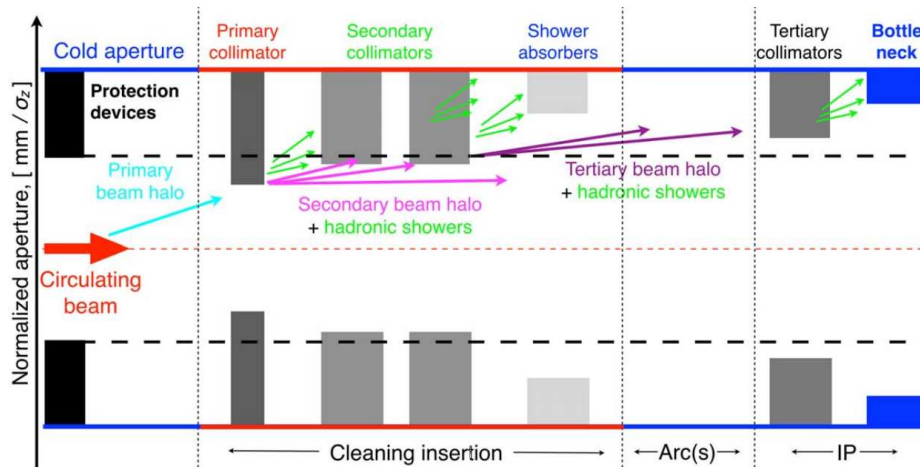
Figure 3: Key elements of the LHC multi-stage collimation system [16]. The TCPs and TCSs are closer to the beam and intercept large beam losses. Therefore, they are made of a carbon fibre composite (CFC) to ensure high robustness. The TCLAs absorb the particles scattered out of the TCSs and the showers from upstream collimators. They are made of a tungsten alloy in order to stop as much as possible of the incoming energy.

A collimation setup comprises a TCP which intercepts beam losses. Its jaws must be set at a transverse aperture below that of the machine bottleneck. However, a single collimator would not be sufficient to clean the beam halo in the LHC, as the halo particles that are scattered before being absorbed by the collimator would leave at larger transverse amplitudes and with different energies. These scattered particles conform the so-called secondary beam halo, which could be lost somewhere in the machine before being absorbed by the collimator in later turns. Moreover, the interactions between the halo particles and the collimator would produce hadronic and electromagnetic showers which could reach sensitive elements if there is not another device to absorb them.

Therefore, the LHC collimation insertions comprise additional collimators downstream the TCPs in order to intercept the secondary beam halo particles.[9] They are called TCSs. Their aperture needs to be larger than in a TCP to ensure that the collimation hierarchy is respected.

An arrangement of TCPs and TCSs in three planes (horizontal, vertical and skew, with

---

[9]The use of "upstream" and "downstream" is related to the direction of the beams. Stating the position of an element as being upstream a certain device indicates that it is located before the device following the direction of the beam.

14

a certain angle) is installed to ensure an efficient cleaning of transverse halo particles. It constitutes a multi-stage collimation cleaning, completed with additional absorbers in order to minimize the hadronic and electromagnetic showers in the cold magnets downstream the collimation region.

This setup still does not guarantee the protection of critical bottlenecks in other insertions. In order to fix this problem, the LHC includes TCTs placed in front of critical machine bottlenecks, as the inner triplets in the experiment IRs or downstream the high-luminosity experiments (ATLAS and CMS) to provide local protection and intercept the collision debris.

In the LHC, the momentum collimation system is located in IR3, before the RF systems in IR4. It corresponds to the insertion where the transverse offset caused by shifts in the energies of the particles is higher. The betatron collimation system is located in IR7.

In case of beam extraction failures, dump protection collimators are installed in IR6. Similarly, there are injection protection collimators in IR2 and IR8.

2.2.4   IR6: Beam Dump Systems

IR6 contains the beam dump insertion. Its function is to extract quickly the beam in a safe way from each ring of the collider and to transport it through a special tunnel to an external absorber, which is a beam stop block made of concrete and graphite composite with different densities. The beam extraction is done using a set of fast-pulsed kicker and septum magnets, which kick the circulating beam and deflect it towards the dump line respectively. A dilution magnet reduces the beam intensity by a factor of $100\,000$ before it collides with the block. Each beam features an independent abort system.

2.3   LHC Cycle

In order to operate the LHC, there is a series of tightly coupled tasks that need to be carried out in strict order and accomplished successfully. This includes for example the machine preparation and injection of the beams, the acceleration to the top energy, the collision of the beams, the beam dump, and the ramp down of the intensity in the magnets after a beam
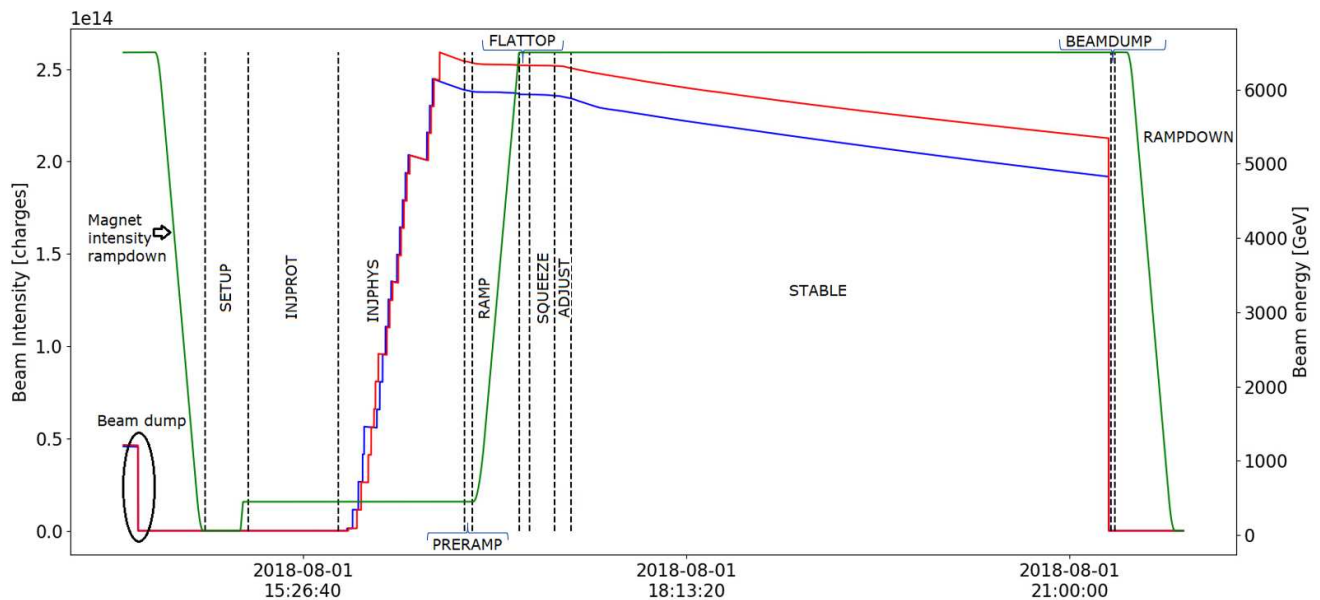
Figure 4: LHC Cycle of a nominal LHC fill, in this case fill 7006. The intensity of Beam 1 and Beam 2 is represented in blue and red, respectively, while the energy of the beams is represented in green. The dashed black lines represent the moments of time in which the beam mode is changed. The name of each beam mode is placed between two dashed black lines: it represents the period of time in which that beam mode is present.

dump. This sequence of tasks constitutes an operation cycle which is called the **LHC cycle**. With every new LHC cycle the so-called **fill number** increases by one.

Depending on the operational activity and the status of the LHC machine, one can distinguish between several so-called **accelerator modes**. These modes provide a summary status and a general overview of the machine activity, and establish the sub-system response [17].

For example, "PROTON PHYSICS" indicates LHC operation with beam aimed at proton physics, while "ION PHYSICS" indicates LHC operation with beam aimed at ion physics. "SHUTDOWN" indicates that the LHC is not operative and some sectors may be cooling down or warming up. The "ACCESS" mode indicates that the LHC is not operative, and access to the machine and/or the experiments is possible.

By contrast, the **beam mode** provides more specific information about the state of the machine, with regard to the main phases of the LHC cycle or sequence which is being played. A nominal LHC cycle regarding the beam modes is shown in Figure 4.

All mode changes are time-stamped and logged in a database. The most common beam modes in an LHC nominal cycle are:

- SETUP: There is possibly beam in transfer lines, not injected in the LHC yet.

- INJECTION PROBE BEAM: Ring 1 or Ring 2 have o will be injected with "probe bunches", safe beam of low intensity. The different accelerator sub-systems are checked before injecting higher intensity beams.

- INJECTION PHYSICS BEAM: The machine is ready to accept higher intensity beams. The full physics production beam (beam used for particle collisions) is injected.

- PREPARE RAMP: The beam injection is complete. LHC systems are being prepared for the energy increase, commonly referred to as "ramp".

- RAMP: The energy ramp is on-going. During this stage the current in the magnets is increased as the energy of the particles does in order to keep the optimal trajectories.

- FLAT TOP: The energy ramp is finished, the particles are at top energy. Some checks are done before "squeezing" the beams.

- SQUEEZE: Preparation or execution of the squeeze of the beams, during which the betatron function (transverse size) of the beams is reduced at the collision points.

- ADJUST: Preparation for collisions or adjust of the beams after the squeeze.

- STABLE BEAM: Both beams have stable conditions with collisions in the experiments.

- BEAM DUMP: Requested or emergency beam dump.

- RAMP DOWN: Ramp down of the intensity of the magnets after a beam dump.

Following the LHC layout and the LHC cycle overview, the highest loss rates are expected to occur in the collimation areas whenever the beam is present in the machine, and the surroundings of the collision points during a stable beam mode, in particular the high-luminosity experiments: ATLAS and CMS. The LHC arcs are expected to be the less radiated regions.

3 BLM System

Due to the high energy and intensity of the LHC beams, the loss of a small fraction of the beam particles could cause either a quench of the superconducting magnets or even physical damage to machine components. A quench of an LHC magnet would generate a downtime in the order of hours. In case of damage, the downtime could be in the order of months in order to replace it [18, 19].

Machine protection has driven the design and implementation of the BLM system, with approximately 4 000 monitors placed along the accelerator to protect the machine equipment against unintended energy deposition by beam losses. The BLM detectors are the main active units of the BLM protection system. In the LHC, the BLM system detects secondary particles from the particle showers produced by beam losses in the accelerator components and generates a beam dump trigger when the losses exceed certain predetermined thresholds [11].

Various mechanisms can lead to beam losses in particle accelerators. Some losses are unavoidable, a result of the standard operation of the machine. Sources of this type of loss are the interactions of the beam particles with the residual gas in the beam pipes, scattering between the beam particles or beam instabilities, among others. However, other losses can be caused by failures of accelerator systems or wrong beam manipulations and should be avoided.

Ideally, all the injected particles would still be present in the stable beams and used for collisions. In reality, part of them are lost elsewhere in the machine. The BLM system helps to identify the loss mechanisms by measuring the loss pattern in the LHC. It allows the observation of local aperture restrictions, system failures and other effects that limit the performance of the LHC. Therefore, apart from the protective function, the BLM system is used for measurements and optimization of the accelerator.

When a beam particle suffers a deviation from its nominal trajectory and interacts with the beam pipe or a magnet cryostat, it can initiate a **particle shower**. Simulations are performed to analyze the development of the particle showers initiated by lost protons in the most likely loss locations. It allows to determine the most suitable number and positions of

the BLM detectors [20].

3.1   BLM Locations and Thresholds

Likely loss locations are those where a large beam transverse size is expected or those with mechanical aperture restrictions. Therefore, there are BLM detectors protecting the quadrupole magnets and after each set of collimators. Other BLM detectors are located in the injection and dump insertions to monitor losses induced by system failures. Furthermore, some BLM detectors are movable to cover unforeseen regions.

The detectors are placed outside the element they are protecting, approximately $1\,\text{m}$ downstream of the most likely loss locations, corresponding to the location of the particle shower maxima. Therefore, the signal given by the detectors is generated by the energy deposition of the particle showers, which is linear with the primary losses. This detector distribution has proven to be the optimal one to localize the losses as well as to distinguish between the two beams [20].

A detector placed outside a quadrupole magnet and another one on the transition between two dipole magnets can be seen in Figure B.1 in Appendix B.

It is essential to relate the BLM signal, generated from the detection of the shower particles, to the primary beam lost protons. This is often calculated considering different loss scenarios via simulation techniques. Further simulations are also performed to determine the energy deposition in machine components from lost protons, as well as the magnet quench levels as a function of the beam energy and loss duration. All these values are often cross-checked and updated with new simulations, measurements in the machine and quench tests.

This information leads to the calculation of the BLM **threshold levels**. Each BLM is assigned a set of threshold levels which is a function of various factors, notably the energy of the beam, the duration of the losses and the position of the monitor itself. If the BLM signal is eventually above one of these thresholds during operation, the beam dump is requested. These values are determined with very high accuracy so that machine protection is ensured without affecting the operational efficiency of the LHC. This includes reducing the number

of "false" beam dump requests, during which the magnets or other machine components are not actually under risk.

3.2   BLM Detectors

Beam losses can have different time duration. Those that occur in a single turn (approximately 89 μs for the LHC) are called ultra-fast losses. Losses that take place progressively during numerous turns can be divided into very-fast losses, which occur in less than 10 ms, fast losses, which take place in more than 10 ms and steady losses, for which the beam is lost in one second or more. For this reason, the losses are recorded under 12 different moving windows known as **RSs**, ranging from 40 μs up to approximately 83.8 s.

Depending on the loss scenario beam losses are expected to be either very small, as at the magnets quench levels, or very large, as at the collimation or dump IRs. In order to cover as many loss scenarios as possible, the BLM system was designed with a high read-out dynamic range of 10^8 of particles fluence[10] to be measured, corresponding to currents generated in the detectors ranging from 10 pA to 1 mA. A dynamic range of 10^{13} at certain locations with higher losses is reached [21].

The main detector type of the LHC BLM system is an **IC**, of which there are approximately 3 600 monitors installed. Figure 5 shows the internal part of an IC. They are made of a stainless steel cylindrical tube, 50-cm long, with a diameter of 9 cm and an active volume of 1.5 l filled with N_2 at an overpressure of 100 mbar. The chamber contains parallel aluminium electrodes plates with a thickness of 0.5 mm equally spaced by 0.5 cm that are alternatively used as high voltage and signal electrodes. A voltage of 1.5 kV is applied between the electrodes, which generates an electric field of 3 kV/cm inside the chamber.

In regions where higher losses are expected, two other types of monitors, **SEMs** and **LICs**, are installed in order to achieve a higher dynamic range and cover the risk of saturation of the ICs electronics.

Both SEMs and LICs have the same geometry and design as the ICs, but their chambers

---

[10]The particle fluence is defined as the secondary particle flux at the location of the detectors, normalised to the number of inducing protons.
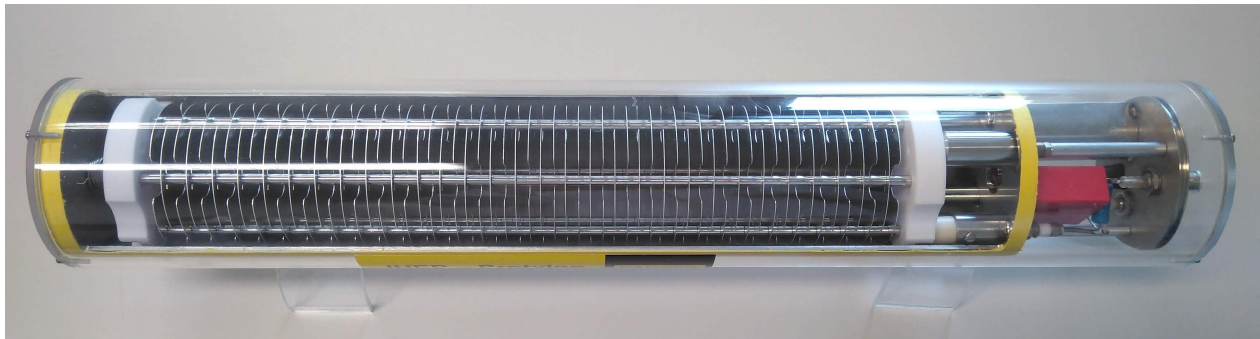
Figure 5: Internal part of an IC BLM showing the electrodes. The cables to the read-out electronics are located on the right part.

are shorter (approximately 10-cm long) and only have 3 electrodes, being the middle one the signal electrode and the other two the high voltage ones. The LICs have in general the same properties as the ICs, but their reduced volume makes them approximately 60 times less sensitive. In contrast, in the SEM detectors the signal electrode is made of titanium to enhance the emission of secondary electrons. Additionally, the SEM chamber is under vacuum, with a pressure below 10^{-7} bar, making it approximately 3×10^4 times less sensitive than the IC detectors [22]. Considering ICs, LICs and SEMs there are approximately 4 000 BLM detectors in total located in the LHC.

3.3   BLM Measurement Principle and Read-out Electronics

The ICs and LICs convert the particle shower caused by mislead protons into an electric current by the principle of ionization. The charged shower particles ionize the N_2 gas inside the chamber as they traverse it. The high electric field applied between the electrodes causes the resulting electrons and ions to drift to the corresponding electrode. This movement induces a signal current with amplitude proportional to the beam loss rate.

The principle of the signal generation in SEM chambers is slightly different. It is based on the secondary electron emission from solids. The path followed by a charged particle through the signal electrode, made of titanium, causes secondary electrons to escape from its surface layers. They are subsequently drifted away as a result of the high voltage applied to the bias electrodes, which induces the signal current [23].
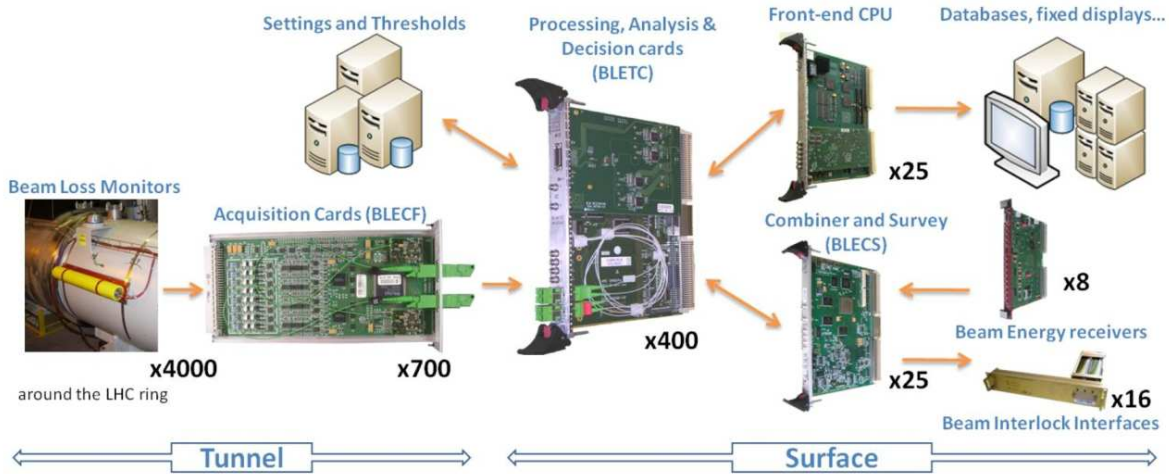
Figure 6: Diagram of the LHC BLM full electronics read-out chain [24].

A diagram of the LHC BLM full electronics **read-out chain** is shown in Figure 6.

3.3.1   BLECF Card

The signals of up to 8 of these detectors are taken to the front-end electronics where they are digitized by the **BLECF card**. These cards are located in the tunnel areas. All components of the tunnel front-end electronics are radiation-certified to $500 \, \text{Gy}$.[11] The BLECF cards located in the arcs are placed in a crate below the quadrupole magnets. In areas with higher levels of radiation, the BLECF cards are placed in crates in separate tunnels, called alcoves. BLECF cards inside their corresponding crates are presented in Figure B.2 in Appendix B. The analog transmission cables that connect the detectors and the BLECF cards are a few metres long in the arcs, but can be up to 500-m long in other areas. This has an impact on the detectors noise levels.

The BLECF cards contain CFCs and ADCs in order to digitize the analog signals coming from the chambers [18]. The basic schematic and principle of the CFC are presented in Figure 7. It includes an integrator made of an Op-Amp and a capacitor with capacitance C

---

[11]The gray (Gy) is the unit of the radiation quantity absorbed dose in the International System of Units. It measures the energy deposited in matter by ionizing radiation per unit mass. It is defined as 1 J of energy absorbed per kilogram of matter [25].
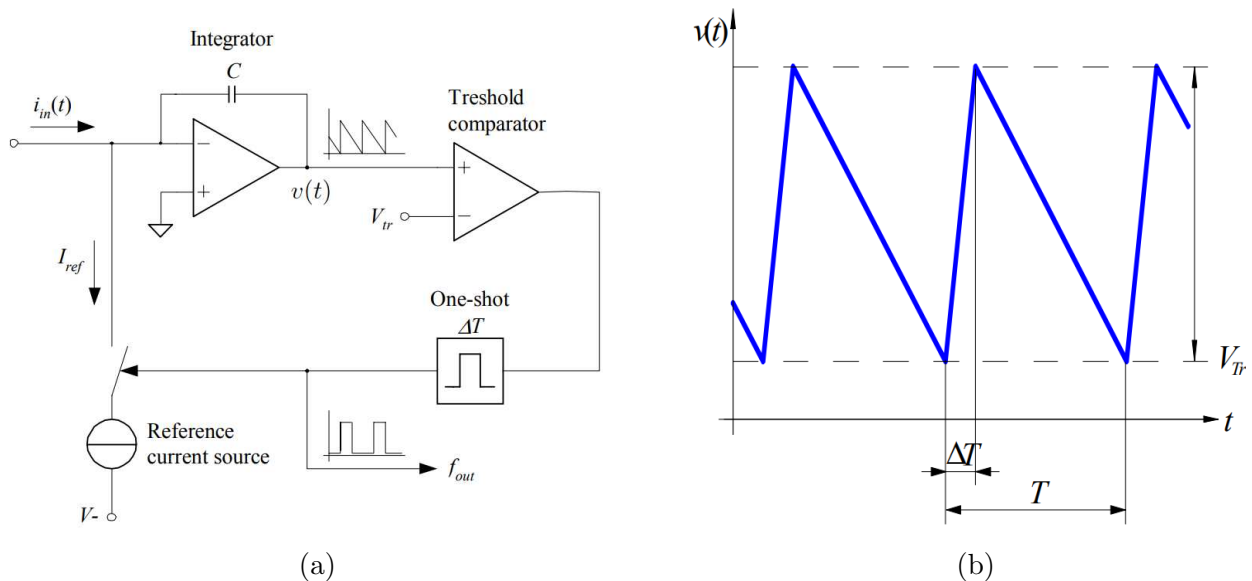
22

Figure 7: (a) Basic schematic of the CFC. (b) Output voltage of the Op-Amp considering a positive and constant signal input current [19].

which is charged by the input signal current from the chamber, $i_{in}(t)$, and discharged by a reference current source, I_{ref}.

If we consider an ideal Op-Amp, with no voltage difference between the inputs and no current flowing in them, $i_{in}(t)$ will be related to the output voltage of the Op-Amp, $v(t)$, as $i_{in}(t) = -C\frac{dv(t)}{dt}$. Considering a positive and constant input current, I_{in}, the output voltage ramps down with a slope that is proportional to the integral of I_{in}, $v(t) = -\int \frac{I_{in}}{C} dt$.[12]

There is a threshold comparator connected to the Op-Amp output that triggers when the value of $v(t)$ reaches a predetermined threshold, V_{Tr}. Following this action a pulse is generated by the one-shot and the reference current source is connected so that I_{ref} is subtracted from the input for a fixed time period ΔT. As it has the opposite polarity and it is larger than the input current, it resets $v(t)$ to its initial value. After this, the reference current is disconnected and $v(t)$ ramps down again until it reaches the threshold voltage. This process is repeated every period T, which depends on the slope of $v(t)$.

In the period T, while the input current is being integrated, a certain amount of charge

---

[12]An ideal Op-Amp is considered to have an infinite open-loop gain, infinite input impedance, zero output impedance and zero input offset voltage. Therefore, the voltage difference between the inputs is supposed as zero as well as the input currents for our calculations.

Q_{in} is accumulated in the capacitor as $Q_{in} = \int_{T} I_{in} dt$. When the reference current source is connected during the reset period ΔT, the induced charge $Q_{ref} = I_{ref} \Delta T$ equals Q_{in}.

The number of resets per unit time defines a frequency that depends on the input current during one period, I_{in}. As $Q_{ref} = Q_{in}$, it can be considered that $I_{in} T = I_{ref} \Delta T$. Therefore, the output frequency is equal to $f = \frac{I_{in}}{I_{ref} \Delta T}$.

The data acquisition and digitization is performed by a counter which measures the number of pulses produced by the CFC and transmits it to the following system every 40 µs. Each pulse is called a **count**. The ADC is employed in order to increase the dynamic range, which is limited by the resolution of the CFC. It directly digitizes the output voltage of the Op-Amp to know the discharge state of the capacitor at the moment when the counter transmits the data from the CFC. With this structure and combining the data from the CFC and the ADC the cases of very slow losses, which generate less than one count every CFC reading, are covered.

3.3.2   BLETC Card

The acquired data are transmitted to a **BLETC card**. The transmission is done by redundant optical fibres in order to improve the reliability and availability of the system. The BLETC cards are located in crates in surface buildings placed on the center of the LHC octants. Thus, the length of the cables ranges from some hundred meters for the BLECF cards in the nearest installations up to 2 km for the BLECF cards located in the middle of the arcs [19].

Each BLETC card is connected to two different BLECF cards, which means it receives the digitized signal from up to 16 different BLM detectors in the tunnel. Each BLM data packet also includes information on the tunnel status, identification of the card and the packet and redundant bits for error detection. The BLETC card combines the counter and ADC data coming from the same detector and merges it into one value.

The BLETC card analyses and keeps a history of these combined data by producing longer integration windows for each signal. These integration windows are the RSs mentioned in Section 3.2. The number of values kept under each integration window defines its width.

The BLETC card compares the result for each new calculation of the RSs of every detector

with the corresponding threshold level. The threshold levels do not depend only on the duration of the loss (considered with each RS) and the detector, but also on the beam energy. This value is provided by the BETS, which calculates it from measurements of the current on the main bending magnets [26].

If any of the RS values of the detectors is above the corresponding threshold level, the card inhibits the beam permit signal, which is sent to the **BLECS** card. After evaluation, it is transmitted further to the BIS to abort the beam. With this scheme and the resolution of the BLM signal it is possible to extract the beam with a maximum delay of approximately 2.7 ms, which corresponds to three LHC turns [11].

The BIS is the backbone of machine protection as it receives status information from approximately 20 subsystems, including the RF and the BLM systems. The beam can be injected in the LHC only if all the subsystems are in a correct state for operation and have sent the beam permit to the BIS. In case one of the subsystems suffers a failure during beam operation and inhibits the beam permit, the BIS triggers the Beam Dumping System [27]. The regular dumps are also transmitted via the BIS.

3.3.3   Logging System

Additionally, the data of the RSs generated in the BLETC cards are continuously stored in the databases by the Logging System at a minimum rate of 1 Hz. For each of the 12 RSs, the logged data include either the maximum value in the 1-s window (up to RS08) or the average value in withing 1 s (from RS09 to RS12), as well as their corresponding threshold values and information on the status of the system [28]. The BLM signal is stored in Gy/s. The packet is read by a CPU which receives the data from 16 BLETC cards located in a crate. Part of these data are constantly displayed in a graphical representation in the Control Room as a diagnostics tool. A permanent storage and data access is provided via the Logging database. A new database system is under development, called NXCALS, planned to replace CALS from Run 3 (starting in 2021) onwards [29]. NXCALS is based on open-source software and will use "Big Data" technologies.

With the purpose of improving the operational efficiency and the performance of the

LHC machine and systems, these data are then used in more sophisticated **offline analysis** of the loss signal developments in the LHC. These studies can help provide information about abnormal high loss locations and foresee failing components, so that interventions can be scheduled in advance. It is also useful for analyzing the integrated radiation dose of the components in the machine.

The data can be queried from CALS via **Timber**, an interactive GUI application. Although Timber has analysis capabilities, it cannot be used in complex data analysis. The Python library **PyTimber** provides an user-friendly tool to extract the data from CALS, including information about the LHC fills and beam modes, beam energy and intensity and the BLM signal of all detectors for the different RSs, among others. These data can then be processed further using Python scripts created by the users.

As an example, the RS09 signal (with 1.3-s integration window) of a BLM detector which protects one of the absorbers located near IP1 was extracted using PyTimber over an LHC cycle and is presented together with the beam energy in Figure C.1 in Appendix C.

A Python library for BLM signal analysis was created as part of this Bachelor's Thesis. The data extraction is done making use of PyTimber. The code source can be accessed via the following link: `https://gitlab.cern.ch/smorales/blm-signal-analysis`. A general description of the code as well as the results of the analysis are discussed in Sections 4,5.

3.4 Reliability Tests

The BLM system is one of the main pillars on which the strategy for LHC machine protection and quench prevention relies. For this reason, it is important to maximize its availability while making sure that the failure scenarios are identified and the status of the system is surveyed continuously. The BLM system has to be fully operational at all moment. Therefore, if the outcome of any of these tests is negative, the beam permit is not allowed in the LHC.

The BLECS card takes care of various checks sequences. Part of these reliability tests are the so-called **sanity checks** which are performed on the system hardware. They are intended to detect non-conformities on the system before a major failure occurs. The sanity checks

have to be performed at least every 24 h [24].

3.4.1   Connectivity Checks

Various tests are part of the sanity checks, but the most relevant one to our study is the so-called **connectivity check**. Its main purpose is to verify the integrity of the cabling of each BLM detector. It is performed by adding a small harmonic modulation signal of 0.06 Hz and 30 V on the high voltage supply of the detector chamber. This modulation of the signal should generate a small current on the measurement side if the connections from the detector chamber to the BLM systems on the surface are correct and functioning properly. If for example the electronic channels of two detector chambers are exchanged, it will be noticed during the check. The BLM system is not operational while the test is running, therefore it is performed during periods with no beam in the LHC. Figure C.2 in Appendix C shows the expected BLM signal during one of these connectivity checks.

The connectivity test also allows to check the integrity of the components by measuring the amplitude and phase of the modulation generated in every channel during the test, and comparing them to a predefined expected value of every channel. In the case the deviation of one of the measured values with respect to the expected value is beyond a certain limit, the beam permit is inhibited and no injections can be done in the LHC.

3.4.2   10-pA Test

The **10-pA test** is always running in the BLECF cards. It aims at monitoring the continuous operation of the acquisition system and the full electronics read-out chain even in the presence of no losses. It consists of a DAC which introduces a constant input current of 10 pA added to the input current from the chamber in the front-end electronics of each detector. This current generates an extra count in the CFC every 20 s. If the BLETC card does not receive a count in 22 s, the input current is then increased by an extra 1 pA. If after 5 consecutive increases of current no counts have been received yet, the detector channel is declared blind and a status signal is sent to the BLETC card to inhibit the beam permit [30].

4 BLM Noise Signal Analysis

In the absence of beam losses, during periods with no beam in the LHC, the BLM detectors still provide a signal value. This is called the BLM **signal offset**. This signal offset is the combination of mainly two components. One is the current of $10\,\text{pA}$ which is connected to the front-end electronics to perform the reliability test explained in Section 3.4.2. It keeps the full LHC BLM electronics read-out chain operating, generating at least one count every $20\,\text{s}$. The other one is the **residual dose** from the activation of the elements around the BLM detector during beam operation in the LHC, causing an increase of the signal in the detectors, which follows a decreasing exponential distribution after a beam dump.

The noise present in the BLM read-out chain can be measured by studying the variation of the BLM signal around the average signal offset value in the absence of beam losses, which is the **standard deviation** of the signal offset.

These two concepts, the BLM signal offset and BLM signal standard deviation, are represented in Figure 8. The figure shows a sample of a typical BLM detector signal in the presence of some perceptible losses during stable beam mode operation. The signal offset level (or baseline) is indicated as well as the standard deviation of the signal and some examples of the signal peaks that can appear in the presence of real beam losses. For the BLM detector signal analyzed, which is one protecting a TCT near IP1, the BLM offset has a value of approximately 3×10^{-7} Gy/s, while the beam losses are at a level between 2×10^{-6} and 4×10^{-6} Gy/s (one order of magnitude higher).

It is important to monitor the value of the signal offset of the detectors at all moment to know which fraction of the BLM signal actually corresponds to beam losses in periods when the particle beams are present in the LHC. Further analysis can be done with the calculated signal offset of the detectors, establishing a comparison between the offset levels in the different regions of the LHC and their evolution in time. This type of analysis allows to detect noisy BLM detectors and schedule the interventions to replace them in dedicated periods, e.g., the so-called **Technical Stops**, minimizing the impact on LHC machine availability.[13]

---

[13]The Technical Stops are planned periods scheduled for maintenance work on the accelerator and experiments. They usually take five days approximately.
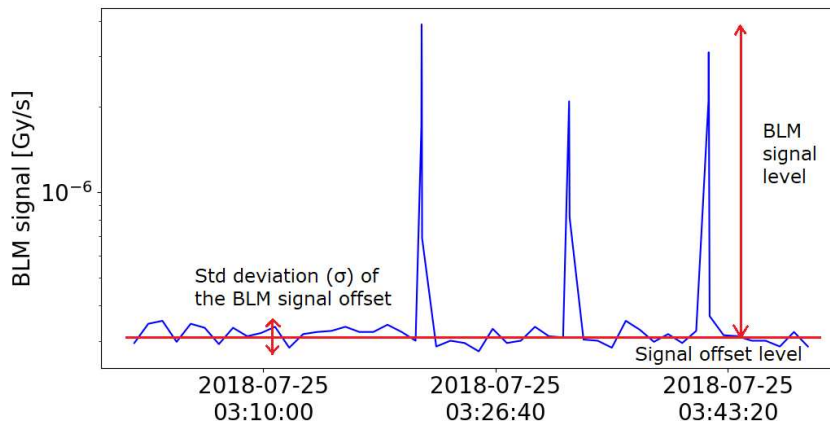
Figure 8: Data sample of a typical BLM detector signal, indicating offset level and its standard variation as well as examples of signal level when beam losses occur.

For these purposes a software analysis module was created and included in the Python library for BLM analysis in order to process the BLM data from Run 2 and calculate the BLM signal offset values of all the LHC BLM detectors in all the periods when the beam was not present in the machine from 2015 to 2018 inclusive. The differences regarding location and time evolution were analyzed, providing as a result a list of the most noisy BLM detectors. The data were extracted making use of PyTimber. The results of this analysis will help determine if any changes on the BLM system are to be foreseen for Run 3 (starting in 2021) and for specific upgrades of the BLM system for the high-luminosity period of the LHC, planned to start in 2027.

4.1 BLM Noise Signal Analysis Methodology

A routine in Python was programmed to calculate the signal offset of all the LHC BLM monitors at different moments during Run 2 (2015-2018). The most complex part of the analysis is to ensure that the data used do not contain any signal from beam losses or from system tests. The code proceeds as follows:

- The information about all the LHC fills is extracted using PyTimber, including the fill numbers, the start and end time of the fills, the beam modes in each fill and their start and end times.
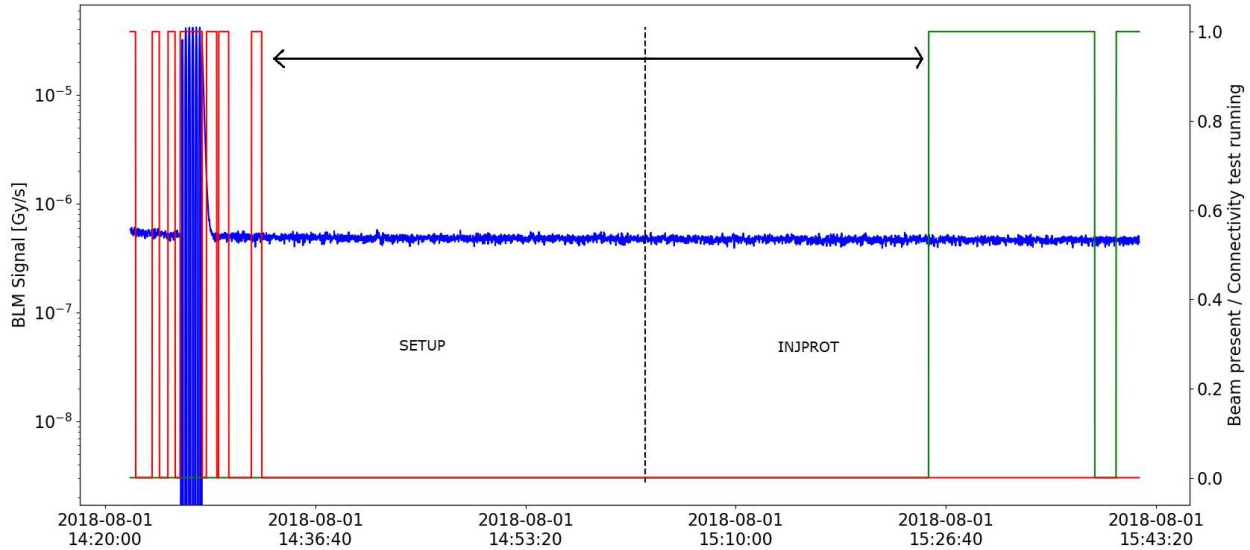
29

Figure 9: Graphical example of the filtering process in the BLM signal offset analysis. The BLM signal is indicated in blue, the boolean variable "Connectivity test on-going" is indicated in red and the boolean variable "Beam present" is indicated in green. Two beam modes, SETUP and INJPROT, are shown. The black arrow indicates the valid period for the filtered data in the present analysis.

- Only the information about the periods during which the beam mode can indicate absence of beam (total or during a partial period) are considered in the analysis, i.e., CYCLING, SETUP, INJPROT and NO BEAM.

- The BLM signal data are extracted from the logging database with RS09 (1.3-s integration window) in the selected periods.[14]

- The extracted data is filtered removing the instants with beam in the machine or reliability tests running, which could bias the signal offset value. A graphical example of the filtering process is shown in Figure 9. Two different beam modes are presented in the figure, SETUP and INJPROT, therefore the BLM signal offset value is calculated separately for each beam mode. The filtered data in the SETUP mode include the BLM signal from 2 min after the end of the test. In contrast, the filtered data in the

---

[14]RS09 is the one selected because its integration time is the closest one to the logging rate (1 Hz) and it is the first RS for which the stored value is the average value of the signal within 1 s, instead of its maximum value.

INJPROT mode include the BLM signal before the injection of the beam in the LHC.

- For each beam mode period selected, the average value (which corresponds to the signal offset value) and the standard deviation of the BLM filtered data of each detector are calculated. If the beam mode period is longer than one hour, as it is usually the case for NO BEAM periods, these values are calculated for every hour within the period.

- The offset value and the standard deviation of the signal of each BLM monitor are saved to a CSV file together with the BLM monitor location in the LHC ring and the information about the corresponding fill and beam mode, among other relevant data.

Therefore, after running this Python routine the full Run 2 is covered with a CSV file per selected beam mode period and per hour within the period with the corresponding data needed for BLM signal offset analysis, thus generating over 7,000 files.

4.2   Measurements of BLM Signal Offset Levels

The calculated signal offset value of all the LHC BLM detectors in October 1, 2018 is presented in Figure 10. The standard deviations of the offset values are indicated as error bars. Each point corresponds to the signal offset level of a LHC BLM detector averaged over the selected period, in this case one day. The x-axis represents the longitudinal position of the detector in the LHC ring. The origin corresponds to IP1 and the position increases as the LHC tunnel is followed clockwise until reaching 27 km, which corresponds again to IP1. The distribution of colours will be the same for the rest of figures showing the three types of LHC BLM detectors, with IC detectors in blue, LIC detectors in green and SEM detectors in magenta.

A baseline (or BLM offset) of approximately 2×10^{-7} Gy/s is observed for most of the IC detectors with the exception of those located in high-radiation areas (collimation systems and experimental IRs) that show a higher value than the average signal offset.

Regarding the LIC and SEM detectors, their offset values are in general higher than the ones of the IC detectors. This was expected because the sensitivity of the detectors is different
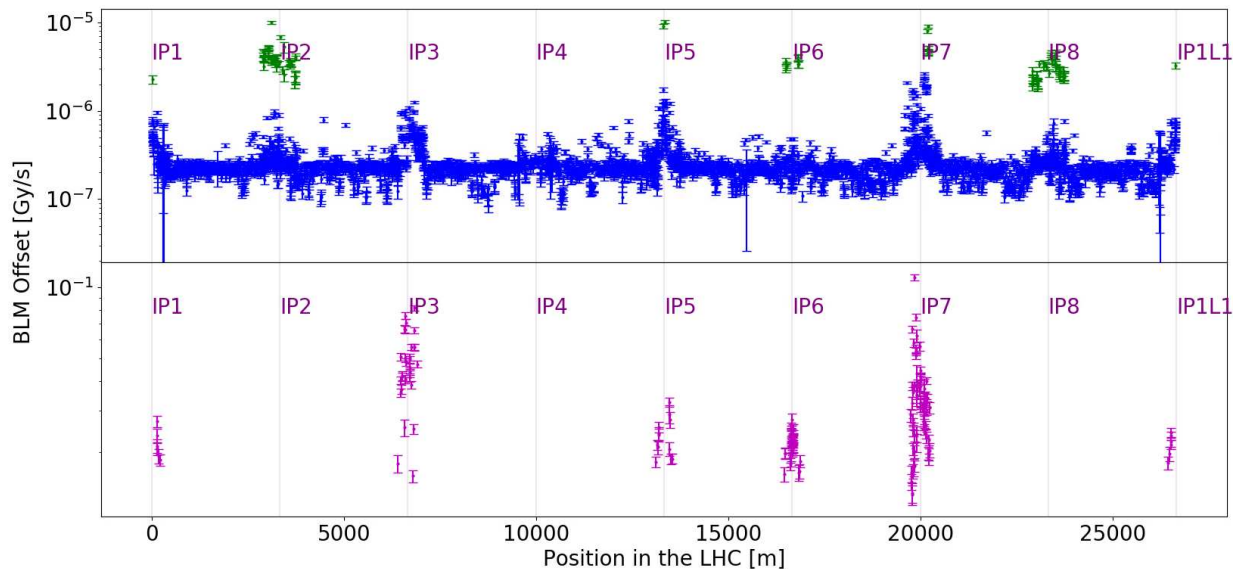
Figure 10: BLM signal offset distribution along the LHC ring for the three types of BLM detectors (ICs in blue, LICs in green and SEMs in magenta). The standard deviations of the calculated offset values are indicated as error bars. The positions of the different IPs are indicated with vertical lines.

and so is the corresponding conversion rate of signal bits to Gy. While for an IC detector a Gy corresponds to 2.76×10^{-9} bits generated in $1\,\mathrm{s}$, for a LIC detector it corresponds to 1.66×10^{-7} bits and for a SEM detector it corresponds to 1.93×10^{-4} bits [31].

4.2.1   BLM Offset Outliers

The reasons why BLM offset outliers appear close to the most radiated areas (collimation systems and experimental IRs) for the IC detectors are analyzed. There are two main effects that contribute to the increase of the IC signal offset in the regions that are highly radiated during LHC operation:

- The aforementioned activation of the surrounding material in the LHC tunnel as a result of the interaction with the proton beam and particle showers. The residual dose of the surrounding material decreases exponentially in the absence of new beam losses. Therefore, this contribution can be studied by monitoring the BLM signal during a physics fill and observing the exponential decay as soon as the beams are dumped. A

precision fit to this decay would potentially provide the contribution of the radioactive nuclei present in the material.

- The Op-Amps located in the BLECF cards suffer from a negative leakage current, which increases with the received radiation dose. To mitigate this effect and ensure a constant input current of at least $10\,\text{pA}$ for the reliability test, active compensation is added using a DAC after a period with high losses [32]. Therefore, this compensation is higher and added more often to the monitors that are located in high-radiation areas. The DAC is usually reset to a lower value during TSs or MD periods.

Considering the nature of these two components, the BLM signal offset is expected to be not only a function of the BLM detector location in the LHC, but also a function of time.

The evolution of the signal offset over the LHC proton operation period in 2018 is presented for two different BLM detectors in Figures 11 and 12. Both figures also show the changes in the compensation value added by the DAC to the CFC input of their respective channels. The detector in the first figure (Figure 11) protects one of the absorbers that intercepts the particle debris from the collisions in IP1, therefore it is located in a high-radiation area. The second one (Figure 12) is located in one of the arcs belonging to the same octant, therefore this is a low-radiation area. The TSs, MDs and Special Physics[15] periods are indicated in the figures.

On the one hand, it is observed that the signal offset of the detector in Figure 11, located in a high-radiation area, experiences large variations between periods of high luminosity in the experiments and therefore high losses, during which it reaches values higher than $10^{-6}\,\text{Gy/s}$, and periods with less operation of the LHC, during which the offset value decays exponentially according to the activation decay of the materials in the tunnel. If these periods are long enough, a stabilization of the signal offset tending to values between $2 \times 10^{-7}\,\text{Gy/s}$ and $3 \times 10^{-7}\,\text{Gy/s}$ is noticeable. On the other hand, the stabilized value depends on the compensating DAC value, which was reset during the 2nd TS (TS2) of the year (17-21

---

[15]Special Physics are planned periods during which the LHC is scheduled to run with low luminosity in the experiments and changes in the beam parameters.
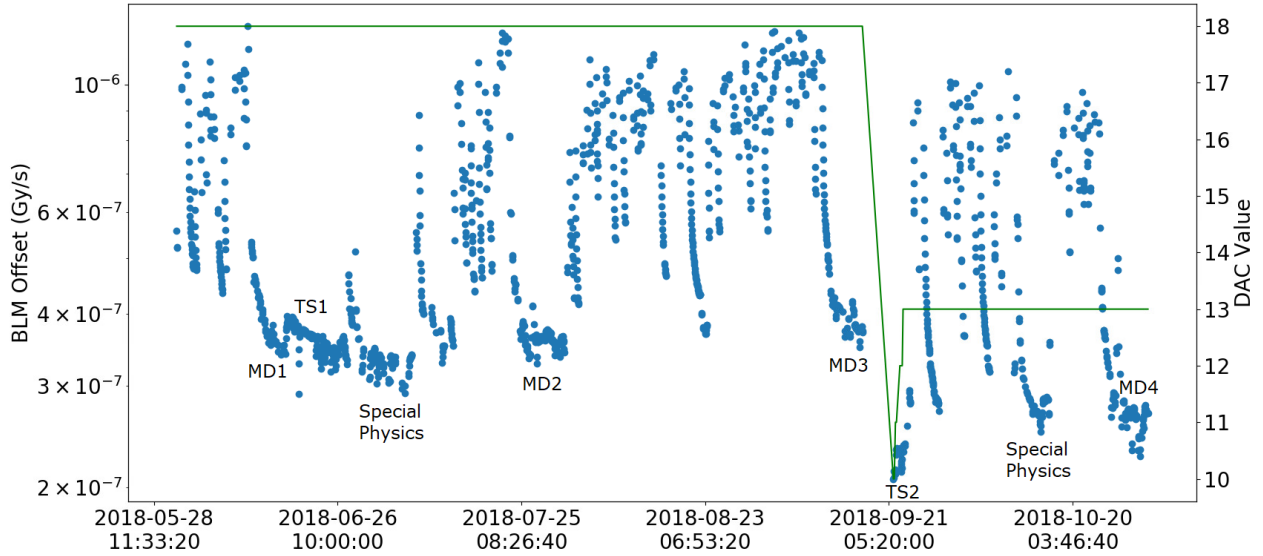
Figure 11: Evolution of the signal offset over time for a BLM detector which protects one of the absorbers near IP1. The signal offset value is indicated with blue points, while the continuous line in green is the compensation DAC value.
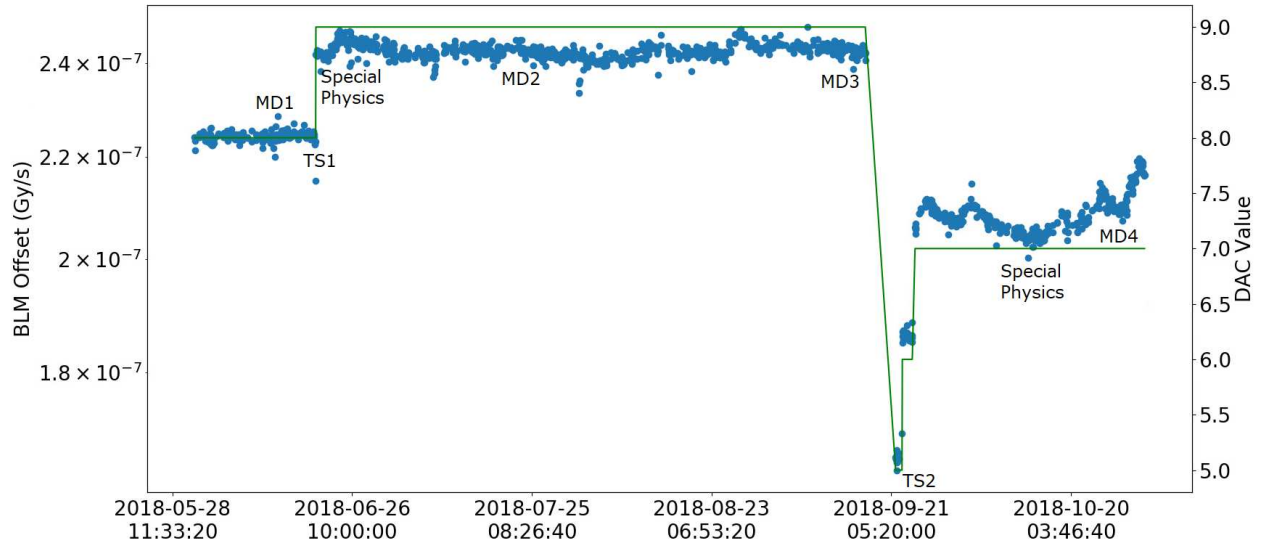

Figure 12: Evolution of the signal offset over time for a BLM detector located in one of the arcs in Octant 1. The signal offset value is indicated with blue points, while the continuous line in green is the compensation DAC value.
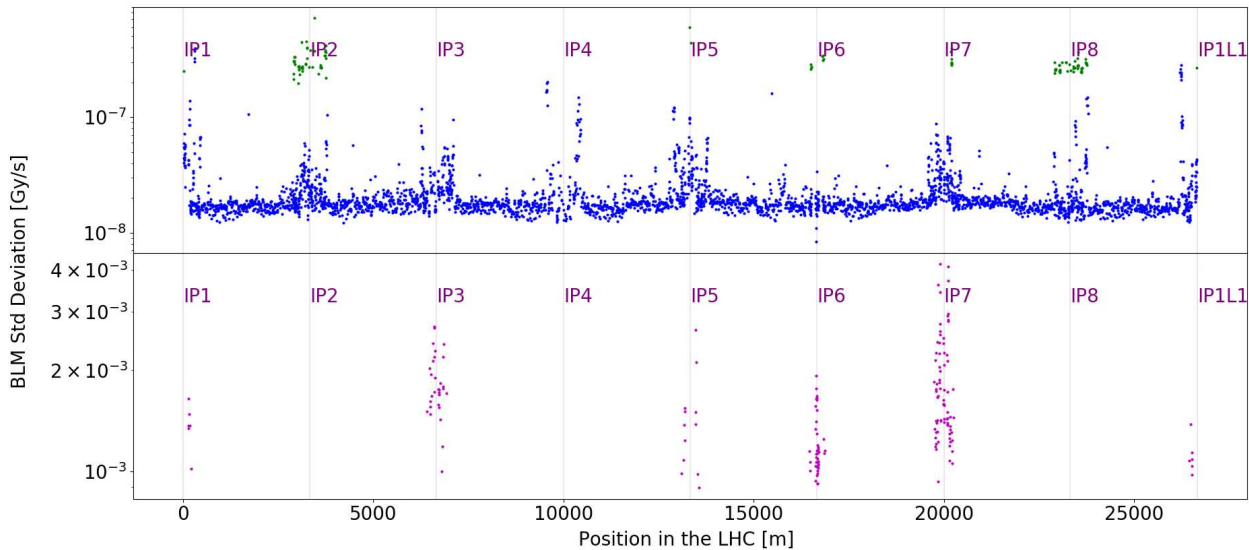
34

Figure 13: Distribution of the standard deviation of the BLM signal offset in the LHC. Each point corresponds to the standard deviation of a LHC BLM detector. ICs are indicated in blue, LICs in green and SEMs in magenta. The positions of the different IPs are indicated with vertical lines.

September) and increased again during the later recommissioning of the machine (22-23 September).

On the other hand, the signal offset value of the detector in Figure 12, located in a low-radiation location, is much more stable during the year, without perceptible changes regarding periods of operation or machine stops. The only relevant variations were due to changes in the compensating DAC value, which was increased during the 1st TS (TS1) of the year (18-21 June) and reset during TS2, increasing again during the later recommissioning of the machine.

4.3   Measurements of Standard Deviation of LHC BLM Signal

As mentioned previously, the standard deviation of the calculated signal offset denotes the presence of noise in the BLM signal read-out chain.

The calculated standard deviation of the signal offset of all the LHC BLM detectors in October 1, 2018 is presented in Figure 13. Notice that now the points represent the fluctuation around the mean value.

It is observed an average fluctuation value of approximately 2×10^{-8} Gy/s for the ICs, with some exceptions. The detectors located near the IPs with higher radiation rates show in general a higher standard deviation. However, these high values are not necessarily due to the presence of noise in the read-out chain. A more detailed analysis of each channel is needed in order to identify the source of high standard deviation values.

As it was described in the previous section, after a beam dump, the signals of the detectors located in these areas decay exponentially according to the residual dose of the surrounding activated materials, tending to the real signal offset value with time. For this reason, the calculated signal offset, which corresponds to the mean value of the signal in the absence of beam losses, will be higher than the baseline in the absence of material activation. Furthermore, as the signal is continuously decaying to the real offset value, its calculated standard deviation will also be higher and not representative of signal noise.

For the sake of better understanding of the effect of the residual dose in the calculation of the offset value and standard deviation of the signal of the detectors, two histograms are presented in Figure 14. They both show the number of CFC counts per second generated in the periods with no beam in October 1, 2018 by the same two detectors in Figures 11 and 12. Figure 14-left (a) shows the data for the BLM detector located in a high-radiation area, while Figure 14-right (b) shows the data for the BLM detector located in one of the LHC arcs belonging to the same octant, a low-radiation area.

The number of CFC counts in the absence of beam should present a Gaussian distribution centered at the value of the signal offset and with a width corresponding to the standard deviation of the signal, dependent on the noise in the read-out chain.

It is observed that for the detector in (a), located in a high-radiation area and therefore with a higher residual dose expected, the number of CFC counts shows larger variations and do not represent exactly a Gaussian distribution. It is observed instead a peak, which corresponds to the real signal offset value, together with a long tail, representative of the decaying signal towards the real value. It is clear that if a Gaussian distribution is considered for this signal, the Gaussian fit will be shifted to the right with respect to the real value, and will show a larger standard deviation which is not a result of the signal noise.
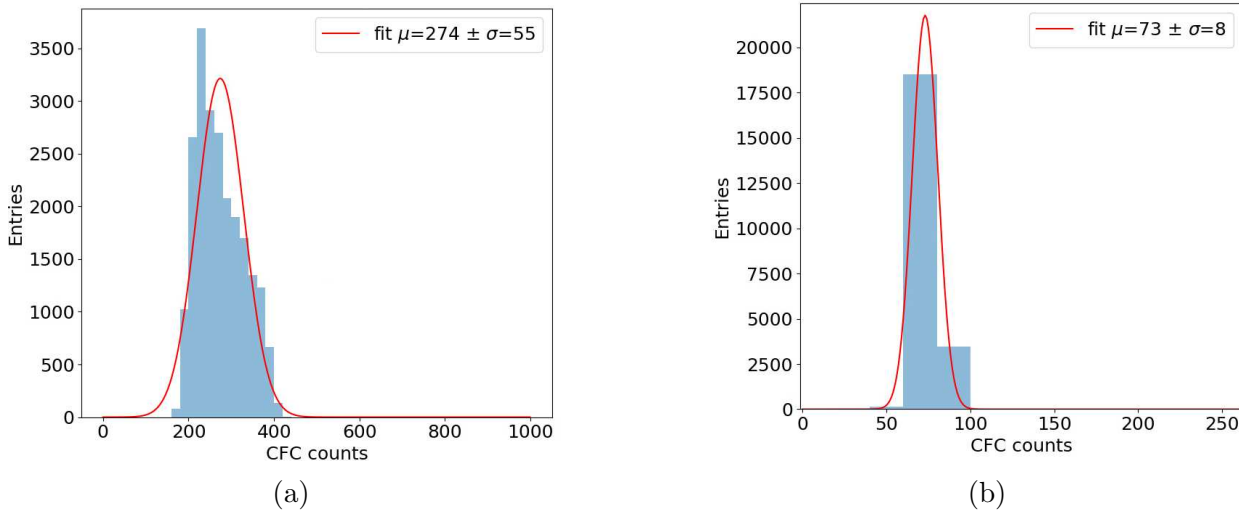
(a) (b)

Figure 14: Histograms showing the distribution of CFC counts per second generated during periods with no beam by (a) a detector located in a high-radiation area and (b) a detector located in a low-radiation area.

In contrast, for the detector in (b), located in a less radiated location, the number of CFC counts is much more stable and follows a Gaussian distribution with lower standard deviation.

Therefore, it makes sense that the detectors with higher calculated offset values due to the residual dose have higher calculated standard deviations as well. However, the fact that some detectors located in low-radiation areas show high standard deviations in Figure 13 must be related to some failure or degradation in the system.

In order to distinguish these noisy detectors from the rest, Figure 15 shows the ratio between the offset and the standard deviation of all the LHC BLM detectors in October 1, 2018.

Although most detectors show an offset-to-standard-deviation ratio of approximately 10, some show a significantly lower ratio. An analysis considering the whole duration of Run 2 was performed to determine the monitors with the lowest offset-to-standard-deviation ratios, and therefore the most noisy BLM detectors.
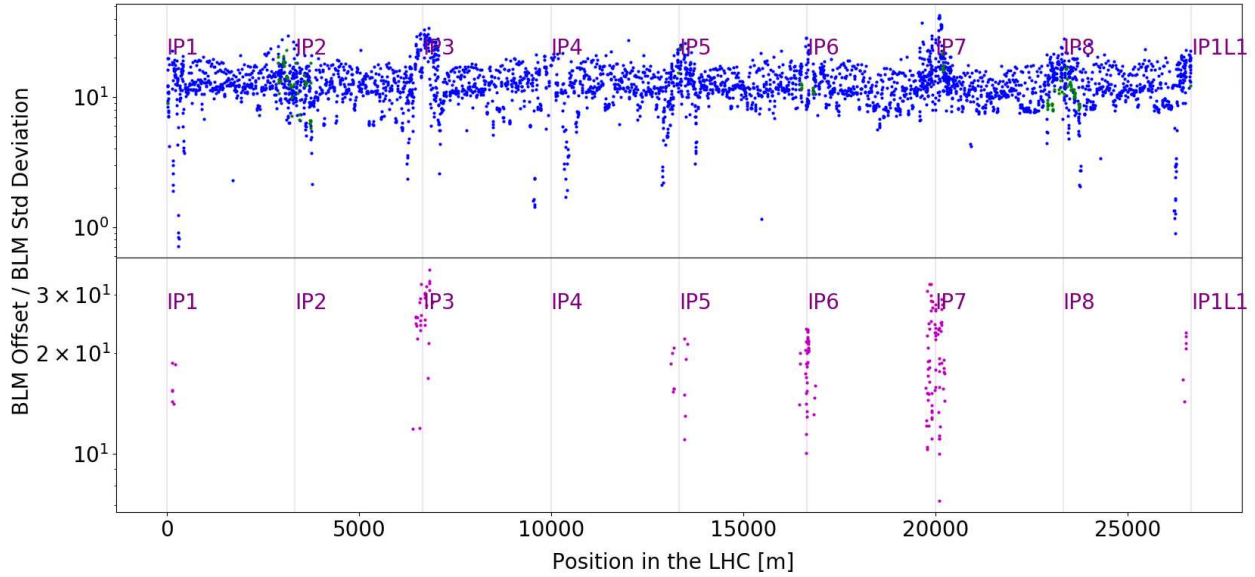
Figure 15: Offset-to-standard-deviation ratio of the LHC BLM detectors. ICs are indicated in blue, LICs in green and SEMs in magenta. The positions of the different IPs are indicated with vertical lines.

4.3.1   BLM Standard Deviation Outliers

After identification of the most noisy BLM detectors, it was observed that they usually appear in groups of between 4 and 6 detectors which are located next to each other and connected to the same BLECF card. Some examples can be noticed easily in Figure 15. Therefore, degraded BLECF cards could be one of the main contributors to BLM signal noise. These BLECF cards are indicated in Table D.1 in Appendix D together with the location of the detectors which are connected to them.

It was also observed that some of these noisy detectors are those located further from their corresponding BLECF cards, and therefore with longer connecting cables. Some actions have already been taken in order to reduce the length of the cables in these cases.

As an example, Figure C.3 in Appendix C shows the BLM signal of two detectors during a NO BEAM period. Both detectors are located in the left DS of Octant 1, but one of the them is connected to a degraded BLECF card. Therefore, its signal is expected to show a higher level of noise.

38

5   BLM Integrated Dose Analysis

A study of the total **radiation dose** received by the BLM detectors during Run 2 is essential to characterize the LHC machine radiation levels, but also to determine if any variations in the BLM signals are expected due to radiation aging of the system.

The total radiation dose received by a BLM detector can be calculated as the integration of the BLM signal over a selected period of time. Since the BLM signal per proton lost in the machine depends on the beam energy, only periods with beams at top energy were considered in this analysis.

The BLM system aging due to radiation effects was studied in the past by analyzing the BLM detectors installed in the SPS. The aging of these detectors was assessed by approaching a ^{137}Cs radioactive source to each of them and reading the generated signal. At the moment of this test the SPS BLM detectors had been in operation for approximately 30 years, during which those installed in the ring had received a radiation dose ranging from 0.1 to 1 kGy per year, while those close to the extraction and injection regions had received a radiation dose ranging from 0.1 to 10 MGy per year [33].

The monitors in the ring, which had received up to 30 kGy in total during the 30 years of operation, showed gain variations below 1%. In contrast, those located in the higher radiation areas, which had received up to 300 MGy in total, showed gain variations of approximately 5%.

Considering the LHC BLM detectors, the highest dose levels need to be assessed. However, it is also interesting to understand how the BLM dose levels (in particular in the most radiated regions) evolve with time and with the different machine parameters such as luminosity or beam intensity, in order to determine if any BLM system limitation is expected for future machine upgrade periods with higher luminosity.

For these purposes a software analysis module was created and included in the Python library for BLM analysis in order to process the BLM data of the full Run 2 and calculate the total radiation dose of the LHC BLM detectors in all the periods when both beams were present in the machine and at top energy (approximately 6.5 TeV) from 2015 to 2018

inclusive. This implies the signal analysis of approximately 4 000 monitors providing data at 1 Hz during 4 years, which constitutes a large amount of data to be analyzed, in the order of TBs.[16]

The dependence of the radiation dose on machine parameters was studied for the detectors in the locations presenting higher dose levels. The data were extracted making use of PyTimber. Similarly to the analysis performed on the BLM noise signal, the results of this analysis will help determine if any changes on the BLM system are to be foreseen for future LHC operation periods.

5.1   BLM Integrated Dose Analysis Methodology

A routine in Python was programmed to calculate the total radiation dose of all the LHC BLM monitors during Run 2 (2015-2018). The code is similar to the Python routine for BLM offset calculation, proceeding as follows:

- The information about all the LHC fills is extracted using PyTimber, including the fill numbers, the start and end time of the fills, the beam modes in each fill and their start and end times.

- However, for this analysis only the information about the periods during which the beam mode can indicate operation of the LHC at top energy (total or during a partial period) are considered, i.e., FLATTOP, SQUEEZE, ADJUST and STABLE.

- The BLM signal data are extracted with RS09 in the selected periods.

- The extracted data are filtered requesting both beams at top energy in the machine. A graphical example of the filtering process is shown in Figure 16. Five different beam modes are presented in the figure, out of which only FLATTOP, SQUEEZE, ADJUST and STABLE are selected for the analysis. In this case, when the machine enters the

---

[16]This value can be obtained with a simple calculation: 4 000 detectors $\times$ 1 stored value per second $\times$ 64 bits per value $\times$ 4 years of operation $\times$ 365 days per year $\times$ 24 h per day $\times$ 3600 s per hour $\approx 32 \times 10^{12}$ bits generated $= 4 \times 10^{12}$ bytes or 4 TB generated approximately in total during Run 2.
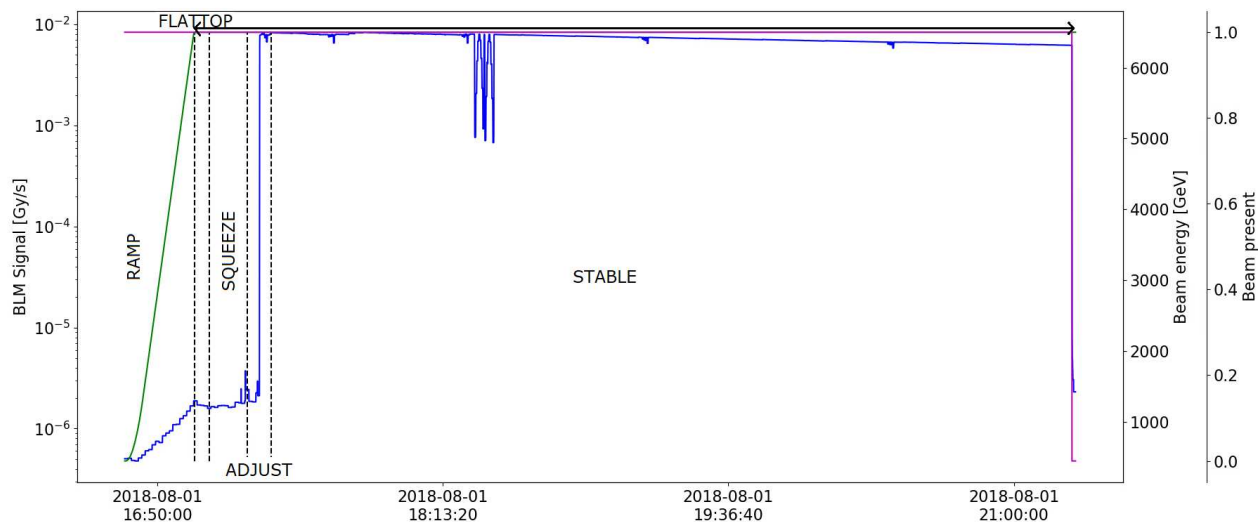
Figure 16: Graphical example of the filtering process in the BLM integrated dose analysis. The BLM signal is indicated in blue, the beam energy is indicated in green and the boolean variable "Beam present" is indicated in magenta. Five beam modes, RAMP, FLATTOP, SQUEEZE, ADJUST and STABLE, are shown. The black arrow indicates the valid period for the filtered data in the present analysis.

FLATTOP beam mode, the beam is already at top energy, therefore the whole period is considered. Similarly, the whole SQUEEZE and ADJUST periods are considered. In contrast, the filtered data in the STABLE mode do not include the BLM signal after the beam is dumped, close to the end of the beam mode.

- For each beam mode period selected, the filtered data are corrected subtracting the closest in time signal offset value calculated. The offset-corrected values are summed to obtain the total radiation dose per monitor.

- The resulting values are saved to a CSV file together with the BLM monitor location in the LHC ring and the information about the corresponding fill and beam mode, among other relevant data.

Therefore, after running this Python routine, the full Run 2 is covered with a CSV file per selected beam mode period with the corresponding data for BLM integrated dose analysis, thus generating over 5 000 files.
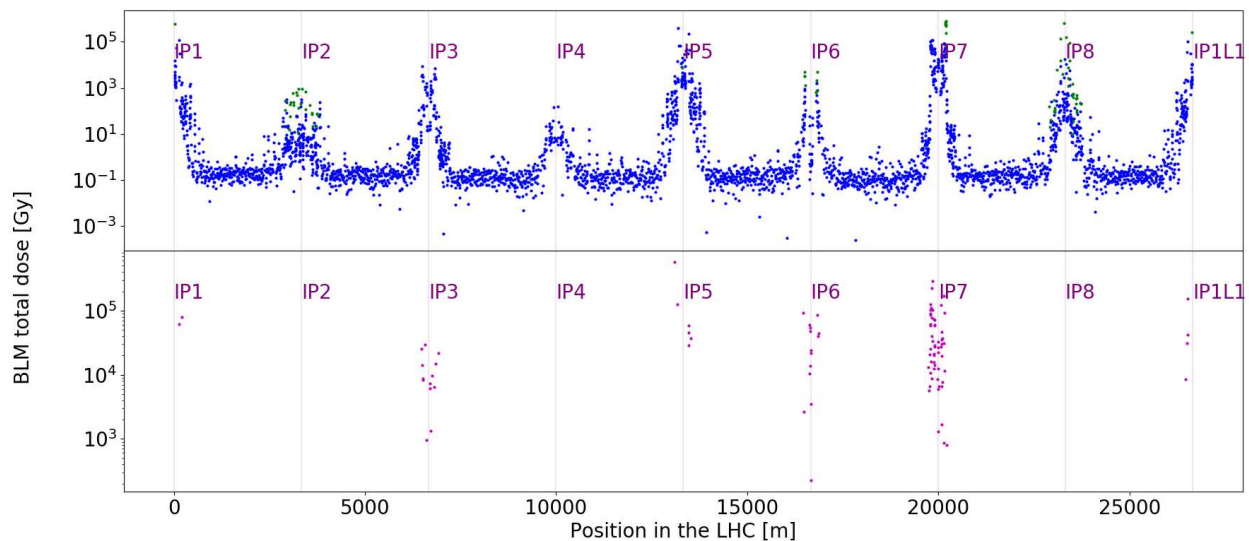
Figure 17: Distribution of the total integrated dose during Run 2 for all the LHC BLM detectors. Each point corresponds to the total integrated dose of a LHC BLM detector. ICs are indicated in blue, LICs in green and SEMs in magenta. The positions of the different IPs are indicated with vertical lines.

5.2   Measurements of BLM Total Integrated Dose

The distribution of the total integrated dose in Run 2 for all the LHC BLM detectors is presented in Figure 17. Each blue point represents the total integrated dose in a particular BLM IC. Similarly in green for the LIC detectors and magenta for the SEM.

A baseline of approximately $0.1\,\mathrm{Gy}$ is observed for the IC detectors located in the arcs. As the BLECF cards located in the crates under the quadrupole magnets in the arcs are radiation-certified to $500\,\mathrm{Gy}$, they are not expected to show any limitation due to radiation aging effects. However, some detectors in the arcs located near their corresponding DSs show dose levels of approximately $100\,\mathrm{Gy}$, thus their corresponding BLECF cards should be followed up closely during the future periods of operation.

As expected, the highest dose rates correspond to the detectors located near the IPs, in particular those located in the experimental IRs with high-luminosity experiments (IR1 and IR5) and the collimation IRs (IR3 and IR7). Some of these detectors reach dose levels of up to $100\,\mathrm{kGy}$, approximately 6 orders of magnitude higher than the baseline at $0.1\,\dot{\mathrm{Gy}}$. The LICs and SEMs show similar dose levels to those of the ICs located close to them.

42

The integrated dose of the most radiated BLM detectors in each IR, distinguishing detectors monitoring Beam 1 and Beam 2 losses are presented in Table E.1 in Appendix E.

There are still significant differences between the highest dose rates in the different IRs. While in IR2, IR4 and IR6 the highest dose levels are in the order between 10^2 and 10^3 Gy, in IR3 and IR8 they are in the order of 10^4 Gy and in IR1, IR5 and IR7 the highest dose levels reach 10^5 Gy. Among them, the highest integrated dose corresponds to a detector which is located in IR5 and monitors the losses of Beam 2. This detector received almost twice the integrated dose of the second most radiated one, which also corresponds to a detector located in IR5, but this one monitors the losses of Beam 1 instead.

5.3   Dose Dependence on Machine Parameters

The dose dependence on machine parameters can be studied for all the LHC BLM detectors. However, as the BLM detectors located in high-radiation areas are the ones which will driven the system limitation, the analysis will be focused on them. This type of analysis is useful to estimate the dose levels expected in the LHC in future periods of operation, and anticipate the changes that will be needed for the BLM system due to radiation aging of the components.

Over all the BLM system, the detectors which received the highest radiation dose during Run 2 are located in the left and right side of IR5, with dose rates of approximately 400 kGy (monitoring Beam 2 losses) and 221 kGy (monitoring Beam 1 losses). In those locations, the received losses are mainly generated from the particle collisions debris. For this reason, a direct relation with CMS luminosity is expected. This is qualitatively shown in Figure 18, where the BLM signal of a detector located close to IP5 (in red) and the instant luminosity in CMS (in green) are presented. It is observed that the BLM signal follows the variations of the instant luminosity in CMS.

A quantitative analysis of this dependence with luminosity is shown in Figure 19. In the figure the integrated dose of the two detectors with the highest dose levels in IR5 is presented as a function of the integrated luminosity in CMS during the whole Run 2. A linear dependence between the integrated dose of these detectors and the integrated luminosity in

Figure 18: BLM signal of a detector located near IP5 and instant luminosity in CMS during a STABLE beam mode period. The BLM signal is indicated in red and the instant luminosity in green.

CMS is clearly observed. Therefore, a regression analysis using the method of the least squares can be conducted with a function of the type $y = ax + b$, where a is the slope of the fit line and b the intercept. The variable x corresponds to the integrated luminosity in CMS and the variable y corresponds to the integrated dose of the detectors. The corresponding lines of best fits are also presented in Figure 19 for the two detectors. The results of the regression analysis are presented in Table E.2 in Appendix E.

This result in IR5 is representative of the rest of BLM detectors located close to the experimental IRs. They also show a linear tendency when performing a study of the dependence of their received dose on the integrated luminosity of the corresponding experiment, as the losses are generated from the particle collisions debris. The slope of the dependency dose-luminosity varies from one detector to the other, being different even for detectors which are located very close. However, dose levels are significantly different between the detectors located in IR2 or IR8 and IR1 or IR5 mainly because of the integrated luminosity in each experiment along the years, which is much higher in IR1 and IR5.

In contrast, in IP7 the losses are mostly generated from the betatron collimation system, which intercepts the beam halo particles with larger-than-nominal transverse amplitudes.
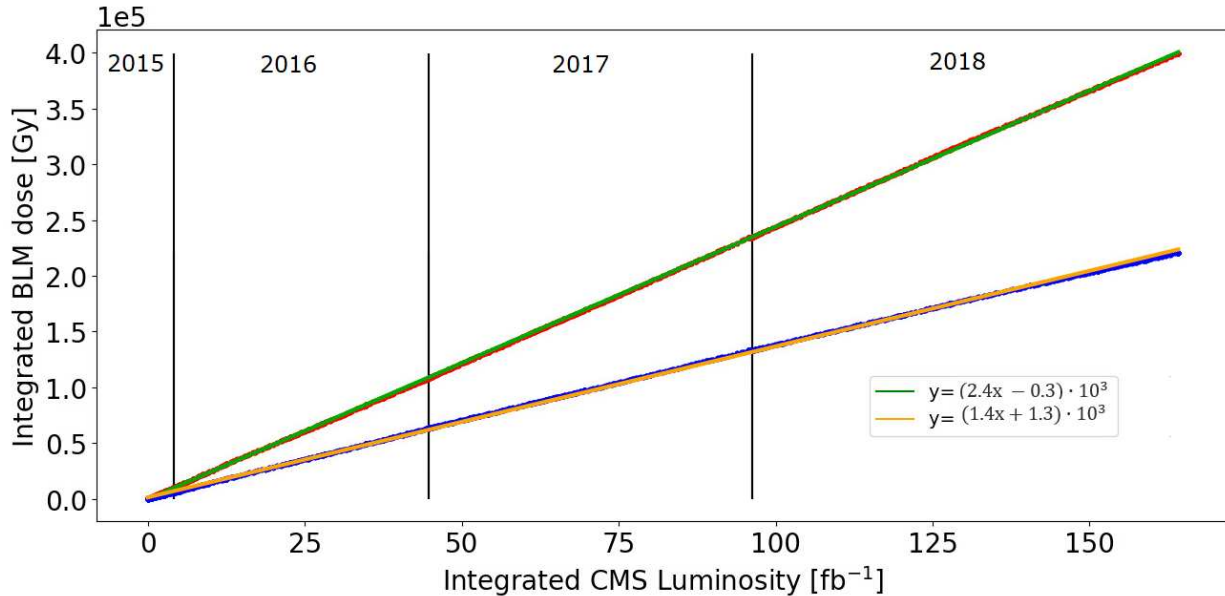
Figure 19: Integrated dose of the two detectors with the highest dose rates in IR5. The detector in blue is the one monitoring Beam 1 losses, and the line of best fit is indicated in green. The detector in red is the one monitoring Beam 2 losses, and the line of the best fit is indicated in orange. The different years of operation of Run 2 are separated by black lines.

Therefore, even though the integrated dose of the most radiated detectors is also of the same order of magnitude, with values of $114\,\mathrm{kGy}$ for a detector which protects a TCS collimator (monitoring losses from Beam 1), and $121\,\mathrm{kGy}$ for a detector which protects a TCLA collimator (monitoring losses from Beam 2), a different analysis is needed. In this case, a direct dependence on the maximum intensity of the beams is expected, as the beam is collimated in these locations and losses from collision debris are further away.

Figure 20 shows the evolution of the integrated dose of the most radiated monitors in IP7 with the integrated maximum intensity of the beams. It is observed that the integrated dose of the detectors increases linearly with the aforementioned quantity, but the slope is not the same during all the years of operation. The slope of both integrated doses in the detectors increased at the start of operation in 2018. This was probably due to a new machine operations configuration.

Considering a linear dependence of the integrated dose of these detectors on the integrated maximum intensity of the beams, a different regression analysis using the method of the least
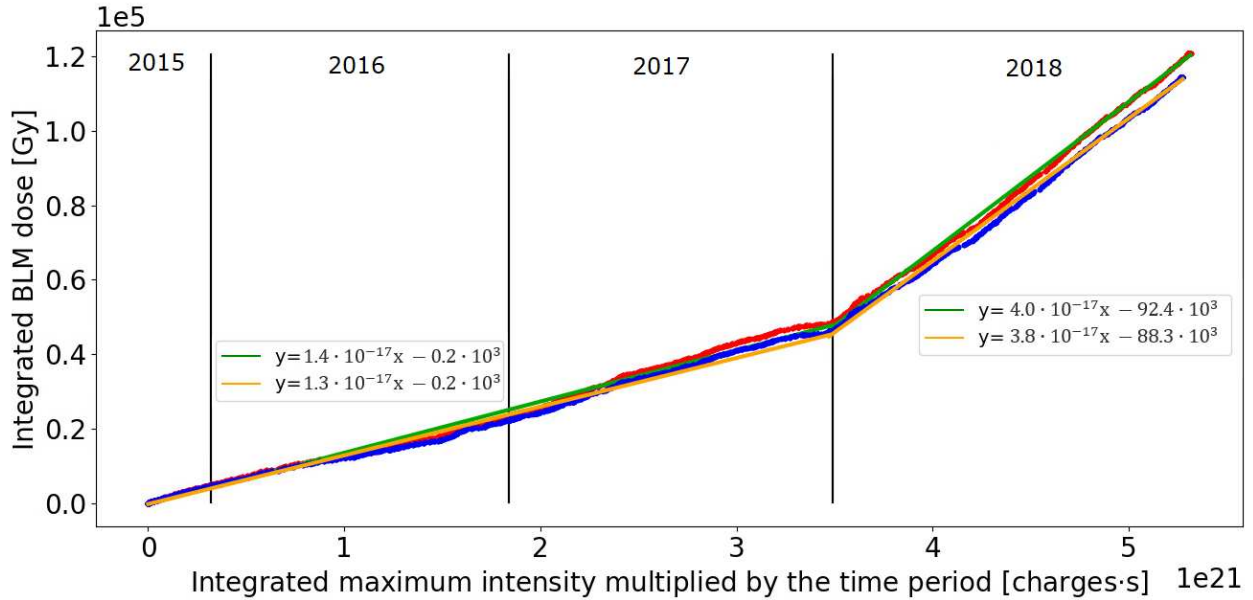
Figure 20: Integrated dose of the two detectors with the highest dose rates in IR7. The detector in blue is the one monitoring Beam 1 losses, and the line of best fit is indicated in green. The detector in red is the one monitoring Beam 2 losses, and the line of the best fit is indicated in orange. The different years of operation of Run 2 are separated by black lines.

squares can be proposed with a function of the type $y = ax + b$ in each of the periods with a similar slope. The variable x corresponds to the integrated maximum intensity of the beams and the variable y corresponds to the integrated dose of the detectors.

For both detectors a regression analysis with parameters a_1, b_1 and R_1^2 is considered for the period 2015-2017 inclusive. A second regression analysis with parameters a_2, b_2 and R_2^2 is considered for the period 2018. The corresponding lines of best fits are also presented in Figure 20. The results of the regression analysis are presented in Table E.3 in Appendix E.

5.4 BLM Integrated Dose in Future Operation Periods

The distribution of the total integrated dose of all the LHC BLM detectors during Run 2 was shown in Figure 17. It was observed that the radiation dose received by some detectors in IR1, IR5 and IR7 in Run 2 is already above the 30 kGy threshold value given by the radiation study explained in Section 5, but far from the 300 MGy threshold value.

According to the LHC long-term schedule, an integrated luminosity of approximately

$300\,\text{fb}^{-1}$ in the ATLAS and CMS experiments is expected for Run 3 [34]. In order to calculate the highest dose rates that could be measured by the end of Run 3, the most radiated detector in IR5 is considered also to be potentially the most radiated detector during Run 3. Additionally for this study, its slope of the dependency dose-luminosity is considered to be the same for Run 2 and Run 3. The calculated value can be found in Table E.2. Taking the $2.4\,\text{kGy/fb}^{-1}$ slope value and multiplying it by the $300\,\text{fb}^{-1}$ expected by the end of Run 3, the corresponding detector would receive an additional $720\,\text{kGy}$ dose approximately.

This would make a total of approximately $1\,\text{MGy}$ dose received by the detector during Run 2 and Run 3, still far from the $300\,\text{MGy}$ threshold value indicated by the radiation study. Following this result, only gain variations between 1% and 5% are to be foreseen for the most radiated detectors by the end of Run 3. However, this result can change depending on the selection of machine parameters.

6 GUI for BLM Signal Analysis

Following the importance of continuously performing an analysis on the BLM signals, including the calculation of the BLM signal offset levels and their integrated dose, a GUI was created as part of this Bachelor's Thesis. Its purpose is to provide an application to anyone willing to use the Python library for BLM signal analysis in a more user-friendly environment. Its code source is also accessible via the link to the aforementioned Python library.

The software Qt Designer was used to design the layout of the GUI, which has then been coded in Python. Figure F.1 in Appendix F shows the layout of the aforementioned GUI.

This GUI allows the selection of any period of time within Run 2, and any of the 12 RSs. The full list of the LHC BLM detectors is provided, with the possibility of filtering by location or type. The option of filtering the monitors by crate, BLETC card, BLECF card or channel within the BLECF card is also given.

Offline signal offset analysis can be performed easily, as the GUI reads the already existing CSV files with the information about the offset values in the selected periods. With only one click the signal offset value of several detectors can be plotted versus time, as well as their standard deviations and the changes in the DAC compensating value. Histograms with the number of CFC counts generated by the detectors in the selected intervals of time can be created, as well as a plot with the signal offset values of all the LHC BLM detectors with respect to their respective locations in the LHC ring.

Offline integrated dose analysis can also be performed, as the GUI has access to the CSV files with the information about the received dose by the monitors in all the periods of time during Run 2. This way, a plot with the integrated dose of all the LHC BLM detectors during a certain period of time can be created. The integrated dose of the BLM detectors can be plotted versus the luminosity in the experiments or the beam intensity for studies on the dose dependence on machine parameters.

The possibility of performing online analysis, directly accessing the logging database from the GUI, is also given.

7   Conclusions

The LHC general structure and systems were described, leading to the conclusion that the areas with the highest dose rates during Run 2 were expected to be the collimation systems and the experimental IRs, in particular those where the high-luminosity experiments (ATLAS, CMS) are located.

The BLM system was presented, highlighting the essential role it plays in ensuring the LHC machine protection and including a description of its main active units, the IC, LIC and SEM detectors. Additionally, an insight on the BLM system read-out electronics was given, from the analog signal generation in the detector chamber to the storage of the digitized data in the logging system, from which it can be extracted to perform offline analysis.

The BLM system has to be fully operational at anytime, and its state needs to be surveyed continuously. In addition to the reliability tests that are performed on the system hardware, the BLM signal must be analyzed thoroughly during LHC operation as well as during machine stop periods in order to detect and anticipate potential failures.

For these purposes, a Python library for BLM signal analysis was created as part of this Bachelor's thesis. It is focused mainly on both BLM noise signal analysis and BLM integrated dose analysis and complemented with the creation of a GUI, which allows to perform the analysis in a more user-friendly environment.

The main structure and functionalities of the codes for the BLM noise signal and BLM integrated dose analysis were described, followed by the presentation of some interesting and useful results from these analysis.

The signal offset of all the BLM detectors was calculated covering the full duration of Run 2. It was observed a baseline of approximately 2×10^{-7} Gy/s with the exception of the detectors located in high-radiation areas, where the residual dose from the activated material in the tunnel and the compensating value added by the DAC to the BLECF card contribute to the increase of the signal offset of the detectors.

This residual dose was shown to be also the responsible for the high standard deviation values of some of the detectors located in these areas. Therefore, a supplementary analysis

of the offset-to-standard-deviation ratio was performed in order to identify the most noisy detectors, which led unexpectedly to the detection of degraded BLECF cards.

The integrated dose of all the BLM detectors was calculated for the duration of Run 2, showing as expected significant differences between the dose levels of the detectors located in the arcs, where a baseline of approximately $0.1\,\text{Gy}$ was observed, and those located in the the collimation systems and the experimental IRs, where some of the detectors reached dose levels of approximately $100\,\text{kGy}$, more than 6 orders of magnitude higher. This result confirmed that no radiation aging is expected in the BLECF cards located in the arcs, which are radiation-certified to $500\,\text{Gy}$. However, those located in the arcs but close to their corresponding DSs should be followed up closely in future periods of operation.

Additionally, an analysis of the dose dependence of the most radiated detectors on machine parameters was performed. It was observed that the dose of the detectors located close to the experimental IPs is linearly dependent on the luminosity of the corresponding experiments, while the dose of the detectors located close to the betatron collimation systems is linearly dependent on the maximum intensity of the beams.

These results were used to determine the maximum dose rates foreseen for future periods of operation of the LHC, concluding that no significant variations in the BLM signal due to radiation effects should be expected.

Appendices

A   2D and 3D Recreations of Accelerator Components

The figures in this appendix show detailed 2D and 3D recreations of the layout of some of the LHC main components, in particular the RF cavities and the superconducting dipole and quadrupole magnets, with the aim of giving an insight into their structure, complexity and operation, as well as providing an idea of their dimensions with respect to the beam pipes.
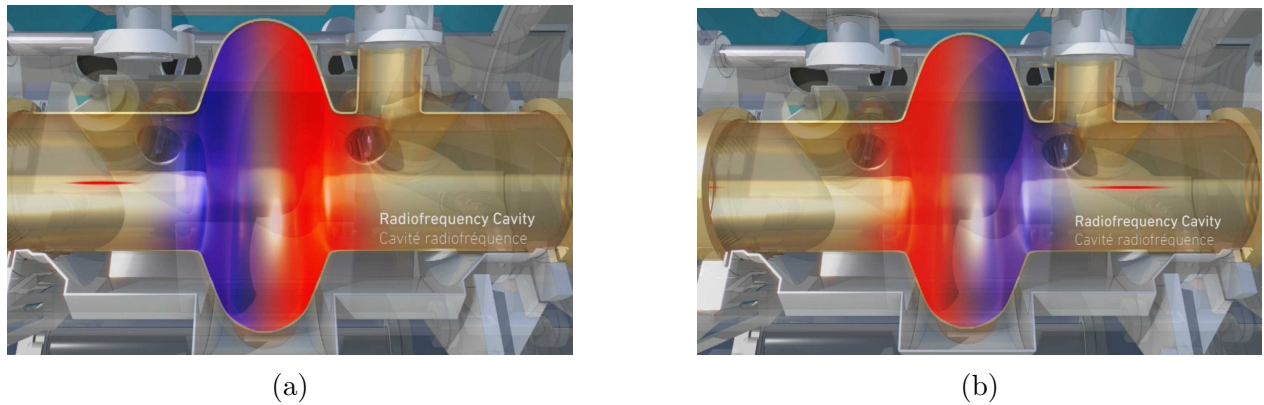

<center>(a)   (b)</center>

Figure A.1: RF cavity. The beam of particles is represented by a horizontal line in red. The electric fields are generated inside the cavity. The direction of the field oscillates according to the arrival of the particles. The red colour represents positive voltage, while blue represents negative voltage. (a) The protons feel attracted by the electric field when they are approaching the cavity. (b) The field changes polarity once the particles have traversed the cavity, repelling them and pushing them forwards along the beam pipes [35].

Figure A.2: LHC tunnel and 3D recreation of the inner part of a dipole (bending) magnet and the beam pipes. The section of the beam pipes is indicated in yellow, and the circulating beams are indicated in red [36].
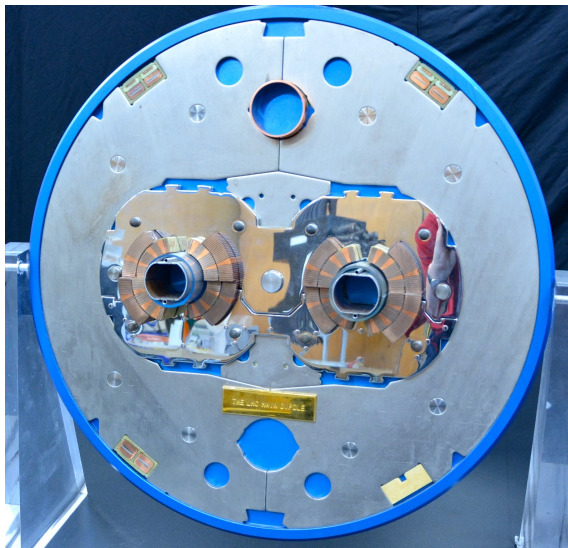
(a)
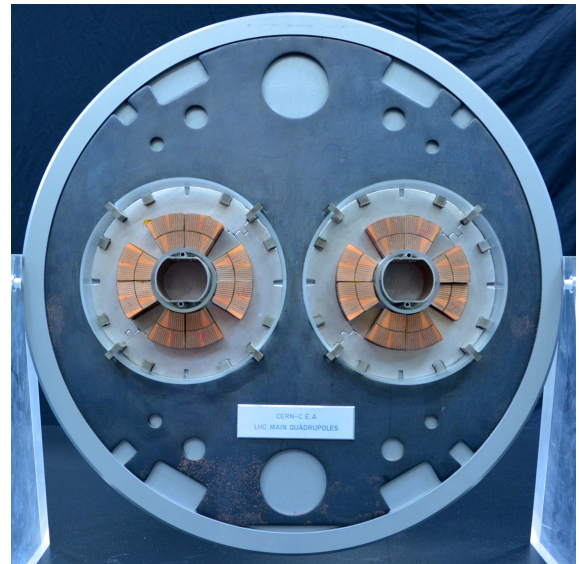
(b)

Figure A.3: Slices through (a) an LHC superconducting dipole (bending) magnet [37] and (b) an LHC superconducting quadrupole (focusing) magnet [38]. Both slices include a cut through the magnet wiring (Nb-Ti), the beam pipes and the steel magnet yokes.

B   BLM System Locations in the LHC Tunnel

The figures in this appendix show the most usual locations and arrangements of the LHC BLM system tunnel instruments, in particular the IC detectors (yellow tubes) and BLECF cards, with the aim of providing a more graphical idea of the BLM system structure.

<table>
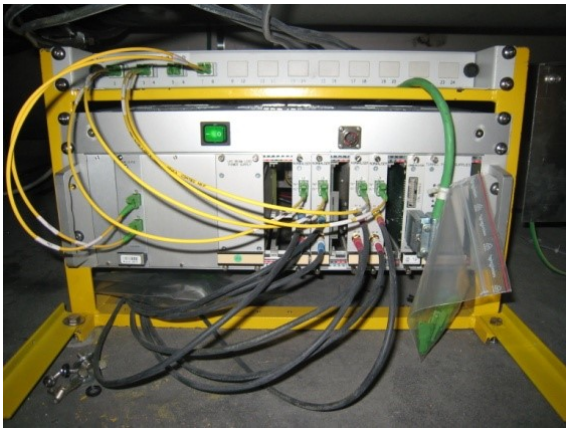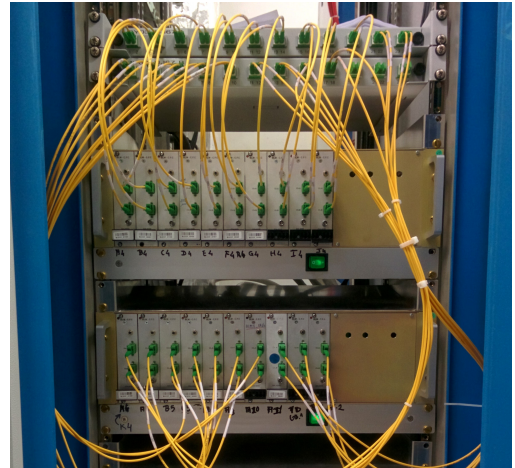<tr><td>(a)</td><td>(b)</td></tr>
</table>

Figure B.1: (a) BLM detectors placed outside a quadrupole magnet. Picture by Lorenzo Stefanini. (b) BLM detector on the transition between two bending magnets [39].

<table>
<tr><td>(a)</td><td>(b)</td></tr>
</table>

Figure B.2: BLECF cards located inside crates (a) in the arcs, under the quadrupole magnets and (b) in the alcoves above the DSs and LSSs. Both pictures by Lorenzo Stefanini.

C   BLM Signal Examples

The figures in this appendix show three interesting examples of variations in the BLM signals that can be observed during normal periods of operation. Each figure is representative of a different effect that produces large and perceptible variations in the BLM signals, as the beam energy and luminosity of the experiments, the performance of a connectivity check on a BLM detector, or the connection to a degraded BLECF card.
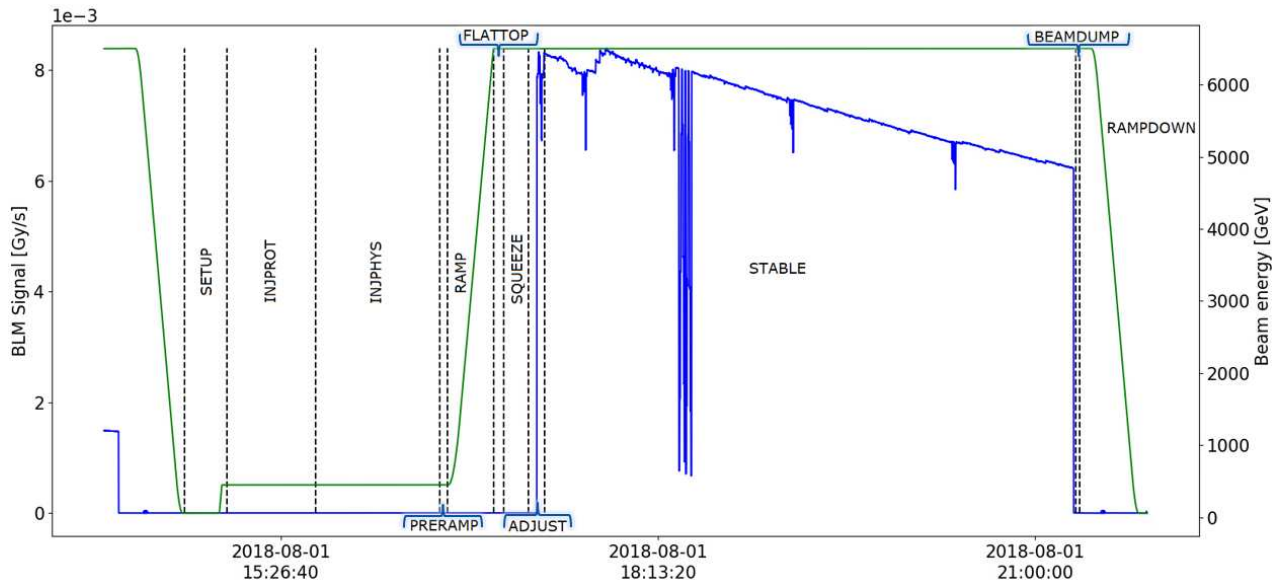

Figure C.1: RS09 signal of a BLM detector and beam energy over the whole duration of the LHC cycle of fill 7006. The BLM signal is indicated in blue and the beam energy in green. It is observed that the BLM signal increases notably during the ADJUST beam mode, probably at the moment when the particle collisions in ATLAS start. The signal decays abruptly after the beam dump. As this detector is located very close to IP1, its signal is expected to be proportional to ATLAS luminosity. Therefore, the changes and the decay in the signal during the STABLE beam mode are most probably due to the variations in ATLAS luminosity, which is adjusted various times during operation and decays with time.
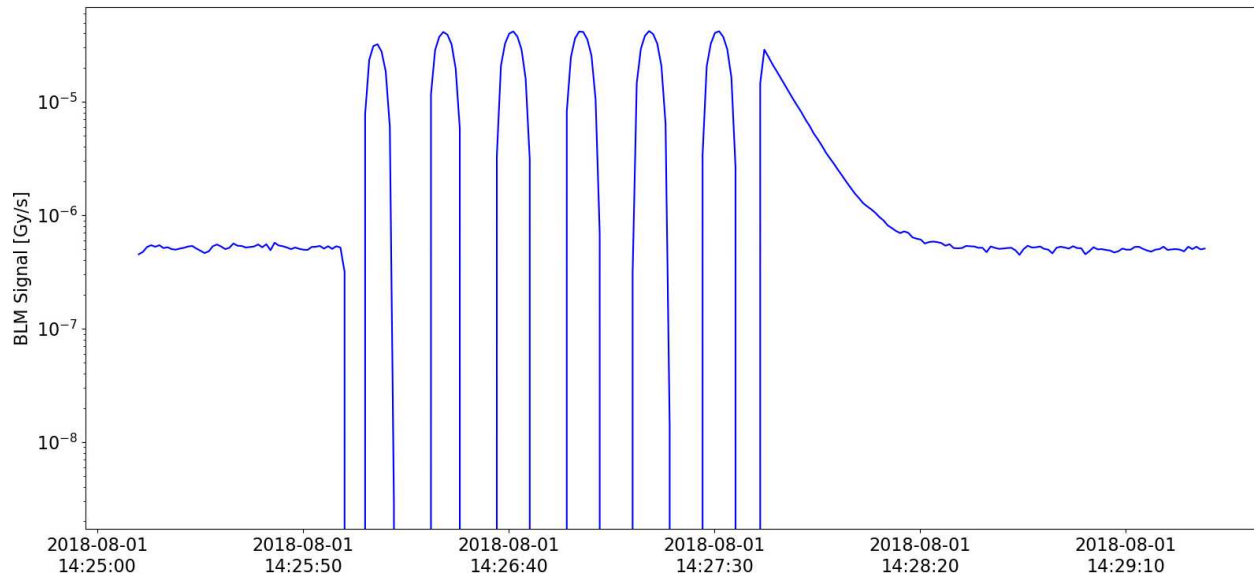
Figure C.2: Standard BLM signal during a connectivity check. The variations in the signal due to the modulation added to the high voltage supply of the detector are highly noticeable.
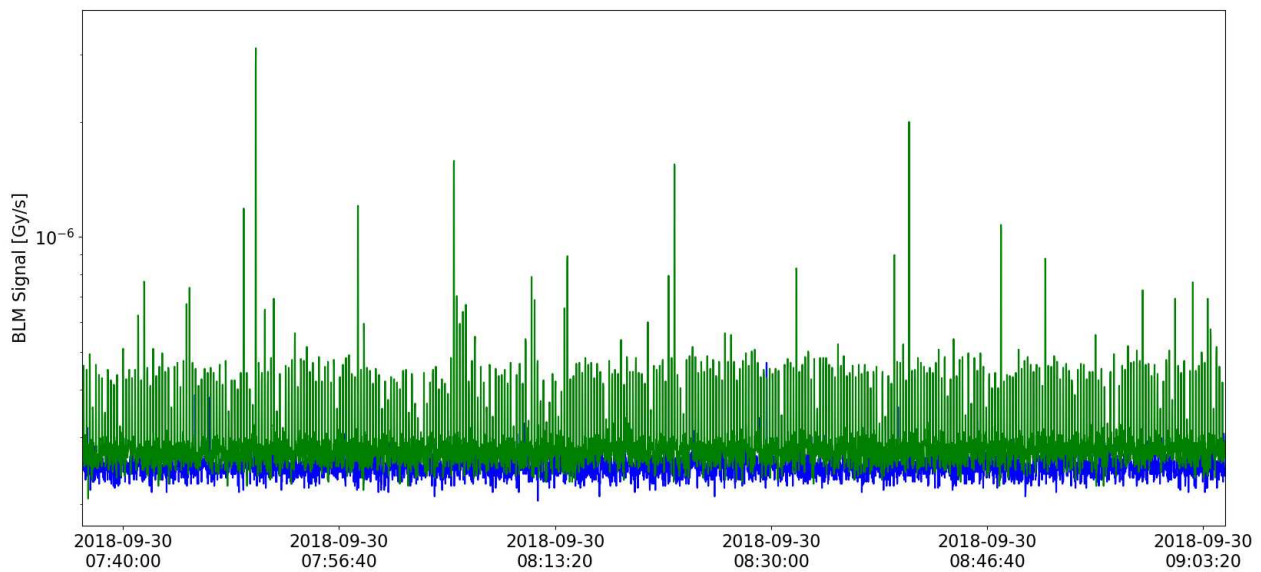

Figure C.3: Signal of two LHC BLM detectors during a NO BEAM period. The signal in green corresponds to a detector connected to one of the degraded BLECF cards. The signal in blue corresponds to another LHC BLM detector located close to the first one, but connected to another BLECF card. Therefore, it is not surprising that the signal of the detector in green shows a higher noise and sudden signal peaks, while the signal of the detector in blue is much more stable and shows less variations.

D   List of Degraded BLECF Cards

In this appendix a table with the results obtained from the BLM noise signal analysis is presented. It shows the number of the degraded BLECF cards as well as the location of the BLM detectors connected to them.

Location	BLECF Number	Location	BLECF Number
Right IP1, LSS	376	Left IP4, Arc	599
Right IP1, DS	647	Left IP4, DS	643
Right IP1, DS	327	Right IP4, DS	509
Right IP2, DS	626	Right IP4, DS	7
Right IP2, DS	627	Right IP4, DS	10
Right IP2, DS	689	Right IP4, Arc	57
Right IP2, Arc	143	Left IP5, Arc	753
Left IP3, Arc	646	Left IP5, DS	581
Left IP3, Arc	607	Left IP5, DS	190
Left IP3, Arc	604	Right IP5, DS	603
Left IP3, Arc	600	Left IP7, Arc	580
Left IP3, DS	654	Left IP8, DS	95
Left IP3, DS	574	Right IP8, LSS	209
Right IP3, DS	562	Right IP8, DS	353
Right IP3, DS	459	Right IP8, DS	39
Left IP4, Arc	616	Right IP8, DS	300
Left IP4, Arc	21	Left IP1, DS	667
Left IP4, Arc	631	Left IP1, DS	594

Table D.1: Location of the most noisy LHC BLM detectors together with the numbers of the BLECF cards they are connected to.

E Highest Dose Rates in Run 2

The following tables show some interesting results obtained from the BLM integrated dose analysis, including the highest dose rates and their dependence on machine parameters.

	Highest dose Beam 1 (kGy)	Highest dose Beam 2 (kGy)
IR1	118.8	102.7
IR2	0.3	0.3
IR3	8.4	6.8
IR4	0.1	0.2
IR5	220.9	399.8
IR6	1.6	0.9
IR7	114.0	120.9
IR8	17.6	10.7

Table E.1: Highest dose rates in the different IRs, distinguishing between detectors monitoring Beam 1 and Beam 2 losses.

	a (kGy/fb^{-1})	b (kGy)	R^2
Beam 1	1.4	1.3	0.9996
Beam 2	2.4	-0.3	0.99998

Table E.2: Results of the regression analysis of the integrated dose of the two most radiated detectors in IR5 with the integrated luminosity in CMS. The parameter R^2 is the coefficient of determination of the regression analysis.

	$a_1 \cdot 10^{-20}$ (kGy/charges·s)	b_1 (kGy)	R_1^2	$a_2 \cdot 10^{-20}$ (kGy/charges·s)	b_1 (kGy)	R_2^2
Beam 1	1.3	-0.2	0.994	3.8	-88.3	0.998
Beam 2	1.4	-0.2	0.994	4.0	-92.4	0.998

Table E.3: Results of the regression analysis of the integrated dose of the two most radiated detectors in IR7 with the integrated maximum intensity of the beams. The periods with different slopes are considered in two different regression analysis for each detector.

F   GUI Layout

The GUI layout is presented, showing in particular a selection of the detectors regarding their connections to the read-out electronics. In this case the GUI is performing a noise analysis of the detectors requested by the user, plotting the evolution of their signal offset values with time together with the compensating DAC value, and histograms of the CFC counts generated by each detector during the selected period of time.
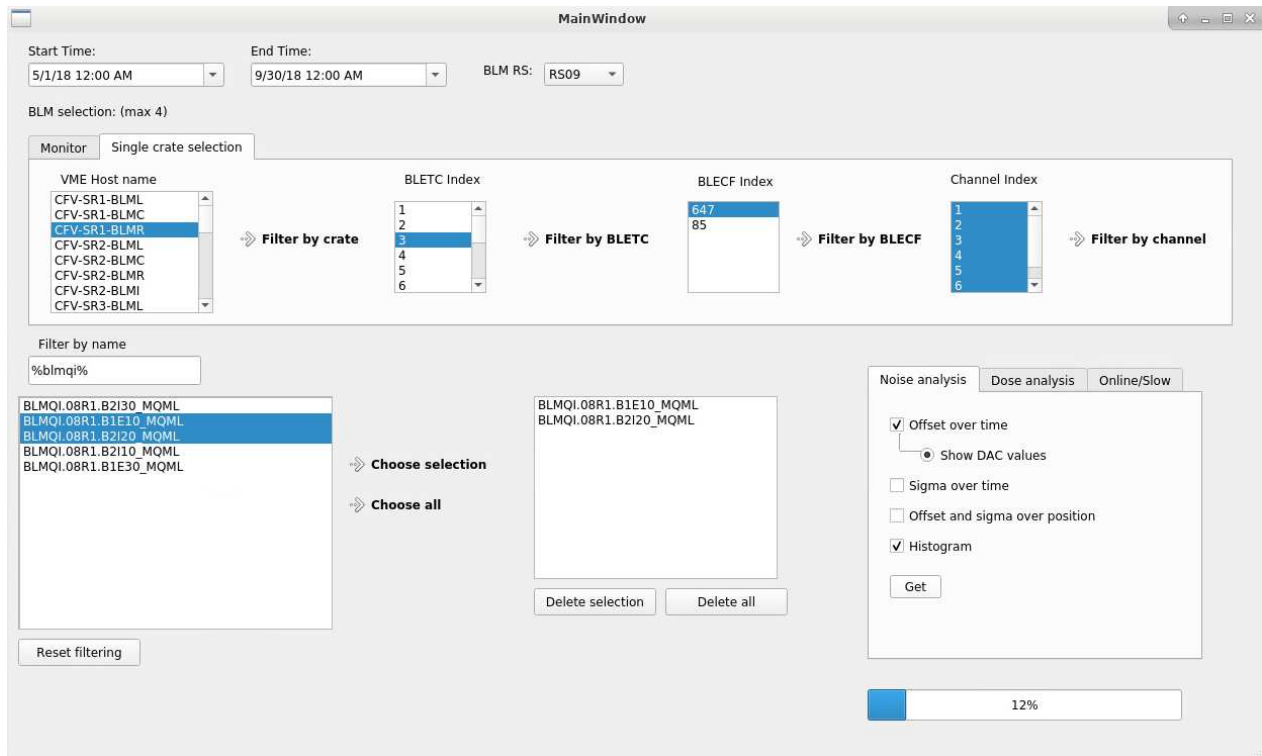

Figure F.1: Layout of the GUI for BLM signal analysis. An overview of the detector selection regarding the connections to the read-out electronics is given, as well as some of the options to perform a BLM signal analysis. A progress bar is included in order to give an idea of the remaining time needed to complete the selected analysis.

References

[1] *CERN official webpage.* URL: https://home.cern.ch.

[2] G. Fidecaro. *The Discoveries of Rare Pion Decays at the CERN Synchrocyclotron.*
     Vol. 23. Adv. Ser. Dir. High Energy Phys. 2015, pp. 397–414. DOI: 10.1142/9789814644150_
     0016. URL: https://cds.cern.ch/record/2103305.

[3] *Radiofrequency cavities.* Sept. 2012. URL: https://cds.cern.ch/record/1997424.

[4] E. Mobs. *The CERN accelerator complex - August 2018. Complexe des accélérateurs du
     CERN - Août 2018.* OPEN-PHO-ACCEL-2018-005. General Photo. Aug. 2018. URL:
     https://cds.cern.ch/record/2636343.

[5] O. Brüning et al. *LHC Design Report.* CERN Yellow Reports: Monographs. Geneva:
     CERN, 2004. DOI: 10.5170/CERN-2004-003-V-1. URL: https://cds.cern.ch/
     record/782076.

[6] *Linear accelerator 4.* Sept. 2012. URL: https://cds.cern.ch/record/1997425.

[7] R. Vanden Broeck. *CCC - SUPER PROTON SYNCHROTRON (SPS). LE SUPER-
     SYNCHROTRON À PROTONS.* Poster-2019-900. Sept. 2019. URL: https://cds.
     cern.ch/record/2694013.

[8] *CERN Annual report 2017.* Tech. rep. Geneva: CERN, 2018. URL: http://cds.cern.
     ch/record/2624296.

[9] J. Wenninger. *Operation and Configuration of the LHC in Run 2.* CERN-ACC-NOTE-
     2019-0007. Mar. 2019. URL: https://cds.cern.ch/record/2668326.

[10] *Restarting the LHC: Why 13 Tev?* June 2014. URL: https://cds.cern.ch/record/
     1998739.

[11] E.B. Holzer et al. *Beam Loss Monitoring System for the LHC.* 2005 IEEE NSS Conf.
     Record. 23-29 Oct 2005, pp. 1052–1056. URL: https://cds.cern.ch/record/930275/
     files/ab-2006-009.pdf.

[12]   *The Large Electron-Positron Collider.* July 2012. URL: https://cds.cern.ch/record/1997351.

[13]   *Pulling together: Superconducting electromagnets.* Aug. 2012. URL: https://cds.cern.ch/record/1997395.

[14]   *LHC Guide.* CERN-Brochure-2017-002-Eng. Mar. 2017. URL: https://cds.cern.ch/record/2255762.

[15]   *The Large Hadron Collider.* Jan. 2014. URL: https://cds.cern.ch/record/1998498.

[16]   S. Redaelli. *Beam Cleaning and Collimation Systems.* 2014 JAS. Newport Beach, CA, USA, Nov. 2014. DOI: 10.5170/CERN-2016-002.403. URL: http://cds.cern.ch/record/2207182.

[17]   R. Alemany et al. *LHC MODES - Functional Specifications.* Tech. rep. LHC Project Document No. LHC-OP-ES-0005. Geneva: CERN, 2007. URL: https://lhc-commissioning.web.cern.ch/systems/data-exchange/doc/LHC-OP-ES-0005-10-00.pdf.

[18]   C. Zamantzas. *The Real-Time Data Analysis and Decision System for Particle Flux Detection in the LHC Accelerator at CERN.* CERN-THESIS-2006-037. 2006. URL: http://cds.cern.ch/record/976628.

[19]   W. Friesenbichler. *Development of the Readout Electronics for the Beam Loss Monitors of the LHC.* CERN-THESIS-2002-028. 2002. URL: https://cds.cern.ch/record/570940.

[20]   E. Gschwendtner et al. *The Beam Loss Detection System of the LHC Ring.* EPAC 2002. Paris, France, 2002, pp. 1894–1896.

[21]   B. Salvachua. *Beam Diagnostics for Studying Beam Losses in the LHC.* Conference Proceedings IBIC 2019, Malmo Sweden, TUAO01.

[22]   V. Grishin et al. *A Family of Gas Ionization Chambers and SEM for Beam Loss Monitoring of LHC and Other Accelerators.* RuPAC 2018. Protvino, Russia, Jan. 2018, TUZMH03. DOI: 10.18429/JACoW-RuPAC2018-TUZMH03. URL: https://cds.cern.ch/record/2674355.

[23] D. Kramer et al. *Simulations and Measurements of Secondary Electron Emission Beam Loss Monitors for LHC*. Vol. 172. Nuclear Physics B - Proceedings Supplements. Proceedings of the IPRD 2007. 2007, pp. 246–249. DOI: `https://doi.org/10.1016/j.nuclphysbps.2007.08.009`. URL: `http://www.sciencedirect.com/science/article/pii/S0920563207006056`.

[24] J. Emery et al. *First experiences with the LHC BLM sanity checks*. Vol. 5. JINST 2010, p. C12044. DOI: `10.1088/1748-0221/5/12/C12044`. URL: `https://cds.cern.ch/record/1321592`.

[25] BIPM. *Le Système international d'unités / The International System of Units ('The SI Brochure')*. Ninth. Bureau international des poids et mesures, 2019. ISBN: 978-92-822-2272-0. URL: `http://www.bipm.org/en/si/si_brochure/`.

[26] R.A. Barlow et al. *The Beam Energy Tracking System of the LHC Beam Dumping System*. ICALEPCS 2005. Geneva, Oct. 2005. URL: `https://cds.cern.ch/record/927409`.

[27] B. Puccio et al. *The CERN Beam Interlock System: Principle and Operational Experience*. Proceedings of IPAC 2010, 2866–2868, WEPEB073. URL: `https://accelconf.web.cern.ch/IPAC10/papers/wepeb073.pdf`.

[28] C. Zamantzas et al. *An FPGA Based Implementation for Real-Time Processing of the LHC Beam Loss Monitoring System's Data*. Vol. 2. IEEE NSS 2006 conference record. Dec. 2006, pp. 950–954. DOI: `10.1109/NSSMIC.2006.356003`.

[29] J.Wozniak et al. *NXCALS - Architecture and Challenges of the Next CERN Accelerator Logging Service*. ICALEPCS 2019, New York, NY, USA. Oct. 2019, WEPHA163. URL: `http://icalepcs2019.vrws.de/papers/wepha163.pdf`.

[30] G. Guaglio. *Reliability of the Beam Loss Monitors System for the Large Hadron Collider at CERN*. CERN-THESIS-2006-012. 2005. URL: `https://cds.cern.ch/record/939785`.

[31] *LHC Software Architecture (LSA) database*.

[32] C. Zamantzas et al. *Real-Time System Supervision for the LHC Beam Loss Monitoring System at CERN*. ICALEPCS 2013, San Francisco, CA, USA CERN-ACC-2013-0255. June 2013, MOPPC062. URL: https://cds.cern.ch/record/1628532.

[33] E.B. Holzer et al. *Development, Production and Testing of 4500 Beam Loss Monitors*. EPAC 2008. Genoa, Italy, 23-27 Jun 2008, TUPC037. URL: https://cds.cern.ch/record/1124309.

[34] *Longer Term LHC Schedule*. URL: https://lhc-commissioning.web.cern.ch/schedule/LHC-long-term.htm.

[35] D. Dominguez et al. *CERN Control Centre Animations 09 "LHC accelerating cavities"*. CERN-FOOTAGE-2014-043-004. Geneva, Aug. 2014. URL: https://videos.cern.ch/record/1750705.

[36] D. Dominguez. *3D cut of the LHC dipole. Coupe 3D du dipôle du LHC*. OPEN-PHO-ACCEL-2014-003. General Photo. July 2014. URL: https://cds.cern.ch/record/1741036.

[37] *Slice through an LHC bending magnet. LHC dipole slice through cold mass*. CERN-OBJ-AC-041. URL: https://cds.cern.ch/record/2284290.

[38] *Slice through an LHC focusing magnet. Tranche quadripolaire LHC à travers la masse froide*. CERN-OBJ-AC-042. URL: https://cds.cern.ch/record/2284291.

[39] M. Kalliokoski et al. *Beam Loss Monitoring for Run 2 of the LHC*. IPAC 2015. Richmond, VA, USA, Mar. 2015, MOPTY055. URL: https://cds.cern.ch/record/2141806.